NASA CONTRACTOR REPORT

NASA CR-1448

THEORETICAL STUDY OF VORTEX SHEDDING FROM BODIES OF REVOLUTION UNDERGOING CONING MOTION

by Gary D. Kuhn, Selden B. Spangler, and Jack N. Nielsen

Prepared by
NIELSEN ENGINEERING & RESEARCH, INC.
Palo Alto, Calif.
for Ames Research Center

NATIONAL AERONAUTICS AND SPACE ADMINISTRATION • WASHINGTON, D. C. • OCTOBER 1969

NASA CR-1448

THEORETICAL STUDY OF VORTEX SHEDDING FROM BODIES OF REVOLUTION UNDERGOING CONING MOTION

By Gary D. Kuhn, Selden B. Spangler,
and Jack N. Nielsen

Issued by Originator as Report No. NEAR TR-14

Prepared under Contract No. NAS 2-4765
NIELSEN ENGINEERING & RESEARCH, INC.
Palo Alto, Calif.

for Ames Research Center

NATIONAL AERONAUTICS AND SPACE ADMINISTRATION

For sale by the Clearinghouse for Federal Scientific and Technical Information
Springfield, Virginia 22151 – Price $3.00

THEORETICAL STUDY OF VORTEX SHEDDING FROM BODIES OF REVOLUTION UNDERGOING CONING MOTION

By Gary D. Kuhn, Selden B. Spangler, and Jack N. Nielsen
Nielsen Engineering & Research, Inc.

SUMMARY

Based on experimental evidence of the existence of a steady asymmetric vortex system on a slender body in coning motion, a theoretical flow model for vortex shedding was developed using potential flow methods and slender-body theory. The model provides for the calculation of the strength and position of each of the two vortices representing the areas of concentrated vorticity in the crossflow plane and the resulting force distribution induced on the body. Initial vortex locations very close to the body must be prescribed to start the computation. For cylindrical bodies, the results for vortex motion and forces were found to be quite sensitive to the initial positions. In order to investigate the nature of the initial condition problem, a linearized analysis of the vortex motion very close to the body was performed. Linearization was found to decouple the motion of the two vortices, so that the paths of the vortices could be obtained, but the relative positions of the two vortices along their paths could not. Upon specializing the body to a cone, it was found that the full nonlinear solution rapidly converged to a unique solution for symmetrical initial conditions, but that the solution was again sensitive to initial asymmetry.

On the basis of agreement with data for a cone and an ogive cylinder in lunar coning motion, the flow model developed is felt to describe reasonably accurately the nature of the vortex-like separated flow over the body and the vortex-induced force distribution. The windward vortex is shown to be somewhat further distant from the body than the leeward vortex and to be somewhat stronger than the leeward vortex over the forward portion of the body. These differences are shown to produce a side force to leeward and a stabilizing side moment in correspondence with the measured results.

The theoretical results were found to be quite sensitive to the assumed location of the separation lines. Accurate knowledge of the

location of separation is required before a truly predictive method can be developed.

INTRODUCTION

The nature of vortex formation on an inclined slender body and its relation to the two-dimensional flow over a cylinder was recognized some 20 years ago (ref. 1). Since then, a considerable amount of both experimental and theoretical work has been done on the nature of the flow over such bodies and the vortex-induced force distribution on them (refs. 2 and 3). It has been only recently, however, that the presence of a steady vortex pair on a slender body in a coning motion has been established (ref. 4). The purpose of the present investigation is to extend certain analytical methods that were developed for the non-coning (planar) problem to the coning problem to examine the nature of the vortex flow and the vortex-induced force distribution on the body.

The coning problem is of importance for spinning bodies which encounter a pitch-roll resonance condition, from which can develop a lunar coning motion (roll lock-in) with unacceptably high angles of attack. The reasons for the development of this type of motion are not well understood. Tobak (ref. 4) has developed a formulation for the aerodynamic moment system in lunar motion which does not depend on constructing the nonplanar motion as the sum of two planar motions. This approach permits coupling of the two planar motions and identifies two types of "Magnus moments": one due to spin about the body axis and one due to rotation of the angle of attack plane (the plane formed by the wind vector and the body axis). The existence of vortices over the body provides a potential source of coupling and nonlinear moments of the latter type. Thus, a method of predicting vortex positions and strengths on a coning body could aid considerably in understanding the nonlinear aerodynamics of lunar motion and the origin of roll lock-in.

The experimental work of Tobak, Schiff, and Peterson (ref. 4 and unpublished data) has shown that a steady, asymmetric vortex system occurs on cones and ogive cylinders in coning motion over a range of angle of attack and Mach number in the low supersonic range. On the

basis of this evidence, slender-body theory is used to construct a potential flow model in the crossflow plane consisting of a pair of vortices whose strengths are not constrained to be equal and whose positions are not required to possess symmetry about any axis system in the fluid. Only the case of lunar motion is considered. The analysis extends to the coning case certain concepts introduced by Bryson (ref. 5) to predict the variation of vortex position and strength along the body and the force distribution induced on non-coning bodies. A linearized analysis is made to determine the initial motions of the vortices very close to the body and the initial development of the vortex strengths. Comparisons with data from reference 4 and unpublished data on slender cones and ogive cylinders are shown to illustrate the nature of the agreement between theory and experiment.

SYMBOLS

a	local body radius
a_o	local radius at base
C_n	side-moment coefficient, $N/q(\pi a_o^2)\ell_o$
C_m	pitching-moment coefficient, $M/q(\pi a_o^2)\ell_o$
C_Y	side-force coefficient, $Y/q(\pi a_o^2)$
C_Z	normal-force coefficient, $Z/q(\pi a_o^2)$
C_{m_q}	stability derivative defined in reference 9
$C_{m_{\dot{\alpha}}}$	stability derivative defined in reference 9
C_{z_q}	stability derivative defined in reference 9
$C_{z_{\dot{\alpha}}}$	stability derivative defined in reference 9
F'	force defined by equation (6)
f_i, g_i	arbitrary functions

ℓ_{cg}	distance from nose to center of gravity
ℓ_o	reference length, distance from nose to center of gravity for cylinder, body length for cone
M	pitching moment about the center of gravity
N	side moment about the center of gravity
p	pressure
q	dynamic pressure, $\frac{1}{2}\rho V^2$
R	real-valued function defined by equation (A-4)
r	radial coordinate of a point in the body-fixed (y,z) coordinate system
t	time
V	free-stream velocity fixed in direction and magnitude
v,w	y,z components of velocity field, respectively
v',w'	y',z' components of velocity field, respectively
W	complex potential
x',y',z'	non-rotating coordinate system with origin fixed at the center of gravity of the body; positive x' directed rearward parallel to the velocity vector, z' in angle of attack plane at t = 0, y' positive direction to form a right-handed system; see fig. 1
Y,Z	components of body force along y,z axes, respectively
Y',Z'	components of body force along y',z' axes, respectively
y,z	rotating axis system in a plane fixed in the fluid perpendicular to the flight velocity vector; origin at intersection of body axis with the fixed plane, z in the angle of attack plane, y positive direction parallel to y' at t = 0; see figs. 1 and 2
α	angle of attack
β	function defined in equation (A-4)
Γ	vortex strength
Γ_m	vortex strength corresponding to an arbitrary circulation of the Magnus type

γ	small angle defined by equation (A-13)
δ	cone half angle
ϵ	non-dimensional distance from feeding point to concentrated vortex
ζ	complex variable, y + iz
ζ'	complex variable, y' + iz'
θ	angular coordinate of a point in the y,z coordinate system
θ_s	angle of separation lines from resultant crossflow vector, defined in figure 3
ρ	fluid density
ϕ	velocity potential; also, angle of coordinate defined by equation (12)
ψ	stream function
ω	magnitude of angular velocity of body about x' axis

Subscripts

c	referred to resultant crossflow
cg	referred to the center of gravity
i	initial value
j	index designating right-hand vortex (j = 1) or left-hand vortex (j = 2)
o	referred to vortex feeding points
v	referred to a vortex center

Conventions

$(\dot{\ })$	time differentiation
$(\bar{\ })$	complex conjugate
ln	abbreviation for Naperian logarithm

PROBLEM DESCRIPTION

A sketch of the motion being considered is shown below.

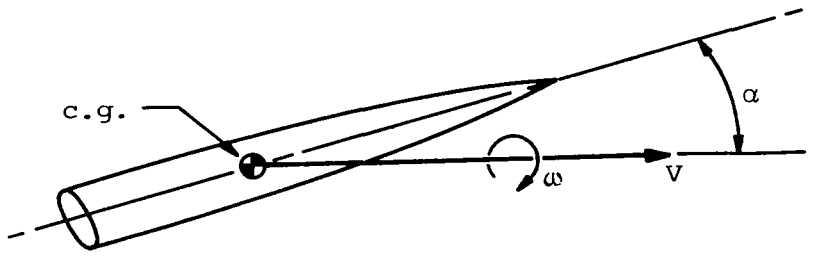

The analysis of the motion is based on the following assumptions:

(a) The body center of gravity traverses a straight path at constant velocity, V, through a constant density fluid.

(b) The body axis is inclined at a fixed angle, α, with the direction of motion of the center of gravity. The body undergoes a coning motion in which the plane defined by the body axis and the velocity vector (the angle of attack plane) rotates at constant angular velocity ω, about the velocity vector.

(c) The body spin rate about its own axis is ω (lunar motion).

(d) The body is axisymmetric.

(e) The angle of attack and Mach number are such that a steady vortex filament pair exists over the leeward side of the body.

EXPERIMENTAL BASIS OF THE FLOW MODEL

An experimental investigation of the flow on a slender ogive cylinder in coning motion was undertaken at the Ames Research Center, NASA (ref. 4). Additional work has been done on both an ogive-cylinder and a slender cone, although the results have not yet been published. The results of these investigations indicate that a steady, asymmetric vortex pair is formed on the body which imposes a significant side force and side moment on the body. The vortex-induced forces are nonlinear with angle of attack and appear essentially linear with the coning rate for fixed angle of attack. The existence of the steady vortex pair forms the basis for the theoretical model and analysis of the present work.

The experimental investigations were conducted in the Ames Research Center 6- by 6-Foot Wind Tunnel at Mach numbers of 1.4 and 2.0 and free-stream unit Reynolds numbers from 1.0×10^6 to 3.5×10^6 per foot. The models were mounted on bent stings which were rotated to produce the coning motion. The vortices were photographed at various axial stations on the body using the vapor screen technique and a camera mounted to rotate with the sting. Variation of the spin rate of the body about its own axis in addition to the coning motion about the center of gravity indicated that for the range of spin rates considered, the spin rate had negligible effect on both the vortex trajectories and the aerodynamic loads on the body.

BASIC THEORETICAL APPROACH

The steady, asymmetric vortex pair observed in the tests described above suggested that the flow model for the coning motion case might be developed in the same manner as the analysis for a slender body at angle of attack. Accordingly, the basic approach followed in this investigation is an extension of the analysis of Bryson (ref. 5) for a slender body at angle of attack. In the real flow, flow separation occurs along two separation lines located on the flanks of the body. Vortex sheets emanate from the separation lines and roll up over the leeward side of the body to form two regions of concentrated vorticity. A steady, three-dimensional flow occurs, as seen in an axis system fixed to the body. Following the notion of Bryson, the two regions of concentrated vorticity over the body are replaced by two potential vortex filaments. The steady three-dimensional potential flow problem is then solved through the use of slender-body theory. According to this theory, the flow can be analyzed in a series of planes along the body axis, where the flow in each plane is unaffected by the flow in other planes. An equivalent model is the unsteady flow in a plane fixed in the fluid through which the body is moving. Thus, the steady, three-dimensional problem can be considered an unsteady two-dimensional flow problem in which time is equivalent to distance along the body. The present analysis is carried out as the unsteady two-dimensional flow in a plane fixed in the fluid and normal to the flight velocity vector. Sketches of this motion are shown in figures 1 and 2.

Figure 1 shows the body piercing the plane fixed in the fluid. An x',y',z' axis system is fixed to the body center of gravity such that the x' axis is colinear with the velocity vector, and the plane formed by the y' and z' axes is parallel to the plane fixed in the fluid. In the plane fixed in the fluid, a y,z axis system is defined, where the origin of the axes is the center of the circle representing the body cross section in the plane and the z axis lies in the angle of attack plane. The body nose is considered to pierce the plane fixed in the fluid at $t = 0$ along the z' axis. Thus, the angle of attack plane makes an angle ωt with the x',z' plane. The two vortex filaments originate at the nose and move away from the body and grow in strength with distance along the body. The vortex strengths are shown in the positive sense (although negative values of Γ_2 are predicted).

The flow model in the plane fixed in the fluid appears as shown in figure 2. The y',z' axes shown are projections into the plane of the actual y',z' axes. The body is rotating with a constant angular velocity ω about its own center. In addition, the body cross section has two translational velocity components: a constant radial component $V\alpha$ and a tangential component proportional to time.

The vortices are considered to be fed from points, ζ_{o_j} on the body, which are the locations of the separation lines on the flanks of the body. The separation points are assumed to have fixed angular relationships with respect to the resultant crossflow vector (vector sum of $V\alpha$ and $\omega V\alpha(t_{cg} - t)$ so that they and the crossflow vector rotate with respect to the y,z system at the same angular rate. The vortex strength at a given vortex position is determined from the condition that the velocity at ζ_o is equal to $\dot{\zeta}_o$. The vortex velocity is determined from a condition of zero net force on the vortex and its "feeding sheet," the latter being a line connecting the vortex to the separation point along which vorticity is considered to be transported. The zero net force condition is an approximation to the exact condition of zero force on each element of distributed vorticity over the leeward side of the body. Using the two above conditions for vortex strengths and velocities and suitable initial conditions for the vortices as they originate at the nose, one can determine the positions and strengths of the two vortices

as a function of time (or distance along the body). From this information the force induced on the body can be obtained.

METHOD OF ANALYSIS

In accordance with the basic approach discussed above, the method of analysis consists of solving for the variation with time of the positions and strengths of the vortices from given initial conditions using two-dimensional potential flow methods. The methods involved are described in this section. The notation and coordinate systems are shown in figures 1 and 2. The x',y',z' coordinate axes are a non-rotating set of axes with the origin fixed at the body center of gravity, whereas the y,z axes are a rotating set of coordinates in the fixed plane. Since the vortex motion analysis is carried out in the y,z system, some care must be taken in dealing with the rotating axis system.

Formulation in the Rotating Coordinate System

In the y',z' coordinate system, the fluid is irrotational and is at rest at infinity. Thus the flow field satisfies Laplace's equation and a velocity potential exists. For motion in the moving (y,z) coordinate system, it is noted that if the coning motion of the body is stopped and all motion is taken with respect to the y,z coordinate system, then there exists a fluid velocity along the positive y axis (horizontal crossflow) proportional to ω and a fluid velocity along the z axis (vertical crossflow) of magnitude $V\alpha$.[1] In addition there is a solid body rotation of the fluid past the body so that the flow field in the y,z system is rotational. The horizontal crossflow velocity is the product of the coning angular rate ω and the distance between the x' axis and the center of the body cross section in the fixed plane. The latter distance is $V(t_{cg} - t)\alpha$, where t is the time measured from the instant the nose penetrates the plane fixed in the fluid and t_{cg} is the time that the body center of gravity moves through the plane. In keeping with the small angle assumption, the body cross sections in the fixed plane are assumed circular to first order.

---

[1] The assumption is made in the analysis that trigonometric functions of α can be approximated with sufficient accuracy by small angle relations; that is, $\sin\alpha \cong \tan\alpha \cong \alpha$, and $\cos\alpha \cong 1$.

Since the flow is irrotational with respect to the y',z' coordinate system, the fluid velocity relative to the y',z' system can be expressed as

$$v' - iw' = \frac{dW'}{d\zeta'}$$

where W' is the complex potential

$$W' = \phi' + i\psi'$$

The fluid velocity relative to the y,z system is

$$v - iw = (v' - iw')e^{i\omega t} - \omega V\alpha(t_{cg} - t) - iV\alpha - i\omega\overline{\zeta} \tag{1}$$

where the last three terms represent the motion of the y,z system relative to the y',z' system. Thus, the fluid velocity relative to the y,z coordinate system consists of an irrotational part, derivable from a potential, plus a rotational part. The fluid velocity in the rotating system is

$$v - iw = -iV\alpha\left(1 + \frac{a^2}{\zeta^2}\right) - \omega V\alpha(t_{cg} - t)\left(1 - \frac{a^2}{\zeta^2}\right) + \frac{a\dot{a}}{\zeta}$$

$$- i\frac{\Gamma_1 + \Gamma_2 - \Gamma_m}{2\pi}\left(\frac{1}{\zeta}\right) - i\frac{\Gamma_1}{2\pi}\left[\frac{1}{\zeta - \zeta_{v_1}} - \frac{1}{\zeta - \frac{a}{\overline{\zeta}_{v_1}}}\right]$$

$$- i\frac{\Gamma_2}{2\pi}\left[\frac{1}{\zeta - \zeta_{v_2}} - \frac{1}{\zeta - \frac{a}{\overline{\zeta}_{v_2}}}\right] - i\omega\overline{\zeta} \tag{2}$$

where Γ represents the strength of a vortex.[2] In equation (2), the first two terms are the crossflow terms. The third term is a source representing the fact that the body radius is changing with time.

[2] In the mathematical formulation, the sign convention on Γ is such that Γ is positive for a counter-clockwise rotating vortex when viewed in the coordinate system shown in figure 2.

For a vortex external to a circle, the circle theorem gives an image system within the circle consisting of a vortex of opposite sign at the inverse point plus a vortex of the same sign at the center (ref. 6, para. 13.50). The fifth and sixth terms, and part of the fourth term, of equation (2) represent the two external vortices and their images. The remainder of the fourth term represents a vortex at the center of the circle of strength Γ_m. The purpose of this vortex is to represent a Magnus circulation that can occur because of the body rotation in the presence of a crossflow. As mentioned previously, experimental results on cones and ogive-cylinder bodies indicated that the aerodynamic loads on the body are insensitive to body spin rate, which implies that the classical Magnus effect is very small. A plausible assumption for the lunar motion case is that the net circulation in the plane fixed in the fluid, which is initially zero, remain zero as the body passes through the plane.[3] Consequently, in the remainder of this report, it has been assumed that

$$\Gamma_m = \Gamma_1 + \Gamma_2$$

The last term in equation (2) accounts for the rotation of the coordinate system.

Solution for Vortex Motion and Strengths

The strengths Γ_1 and Γ_2 of the vortices, for given positions ζ_{v_1} and ζ_{v_2}, can be determined from the condition that the fluid velocities relative to the moving separation points at ζ_{o_1} and ζ_{o_2} are zero. Thus,

$$\left\{v - iw\right\}_{\zeta_j=\zeta_{o_j}} = \dot{\bar{\zeta}}_{o_j} \qquad j = 1,2 \tag{3}$$

This condition supplies two equations for the two unknowns Γ_1 and Γ_2.

The condition for zero net force on a vortex and its "feeding sheet" can be formulated by observing that the force on the external vortex is equal and opposite to that on the "sheet." The force on an external vortex is $i\rho\Gamma(\dot{\zeta}_v - V_v)$, where V_v is the velocity induced at the

[3]Some other condition might also be invoked to determine Γ_m, e.g., that some specified point on the circle become a stagnation point, as in the case of the Kutta condition applied to an airfoil mapped into a circle.

vortex by all components of the flow other than the vortex itself, and $\dot{\zeta}_v - v_v$ is the vortex velocity relative to the local induced flow. A force exists on the sheet because of the rate of change of strength of the concentrated vortex. The force on the sheet is thus determined from the unsteady Bernoulli equation applied to the irrotational flow around a vortex as follows. Consider a vortex of strength $\Gamma(t)$ at the origin of a coordinate system as shown in the following sketch.

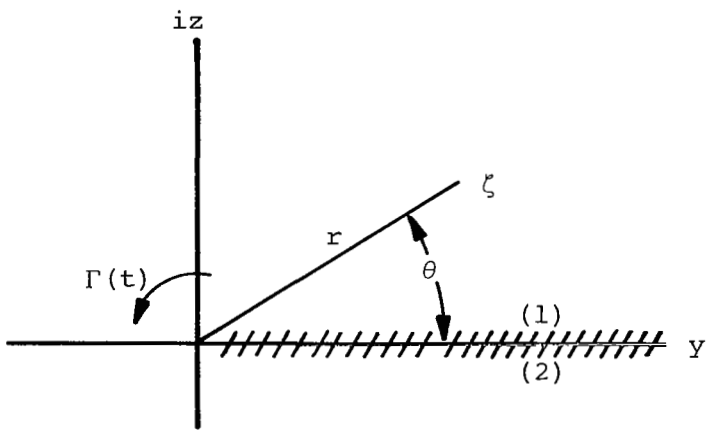

The complex potential for this vortex is

$$W_v = \phi + i\psi = -i \frac{\Gamma(t)}{2\pi} \ln \zeta = -i \frac{\Gamma(t)}{2\pi} (\ln r + i\theta)$$

Therefore, the velocity potential is

$$\phi = \frac{\Gamma(t)}{2\pi} \theta$$

and

$$\dot{\phi} = \frac{\dot{\Gamma}(t)}{2\pi} \theta$$

In order for the velocity potential to be single-valued, a branch cut must exist which in this case is indicated along the positive y-axis from $y = 0$ to $y = +\infty$. Thus, the value of θ is limited to the range of zero to 2π. There is a discontinuity in ϕ across the branch cut of value $\Gamma(t)$, but the velocity is continuous across the branch cut.

The unsteady Bernoulli equation (para. 3.60, ref. 6),

$$\frac{p}{\rho} = \frac{-1}{2}(v^2 + w^2) - \frac{\partial \phi}{\partial t} + C(t)$$

when used to obtain the pressure difference across the branch cut yields the result

$$p_1 - p_2 = \rho \dot{\Gamma}(t)$$

In the case of the vortex and its image as shown in figure 2, the branch cut can be considered to be a line joining the external vortex to its image. The cut is assumed to pass through the separation point ζ_o on the body so that the portion of the cut external to the body coincides with the sheet. The net force on the sheet is then the product of the pressure difference across the sheet and the length of the sheet.

Thus, the force balance relation for each vortex is

$$i\rho\Gamma_j(\dot{\zeta}_{v_j} - V_{v_j}) + i\rho\dot{\Gamma}_j(\zeta_{v_j} - \zeta_{o_j}) = 0 \qquad j = 1,2 \qquad (4)$$

In this equation, Γ_j is a known function of ζ_{v_1}, ζ_{v_2}, ζ_{o_1}, and ζ_{o_2} (from eq. (3)) and $\dot{\Gamma}_j$ can be obtained by time differentiation of the expression for Γ resulting from equation (3). Thus, the only unknown is the vortex velocity $\dot{\zeta}_{v_j}$. Equations (1) through (4), after some algebra, yield a set of simultaneous first-order differential equations, linear in the derivatives, $\dot{\zeta}_{v_j}$. These equations are of the form

$$\begin{aligned} f_1\dot{\zeta}_{v_1} + f_2\dot{\bar{\zeta}}_{v_1} + f_3\dot{\zeta}_{v_2} + f_4\dot{\bar{\zeta}}_{v_2} &= V_{v_1} - g_1 \\ f_5\dot{\zeta}_{v_1} + f_6\dot{\bar{\zeta}}_{v_1} + f_7\dot{\zeta}_{v_2} + f_8\dot{\bar{\zeta}}_{v_2} &= V_{v_2} - g_2 \end{aligned} \qquad (5)$$

where the f_i and g_i are complex valued functions of ζ_{v_1}, ζ_{v_2}, ζ_{o_1}, and ζ_{o_2}.

The equations for the vortex motion (eq. (5)) are to be solved for given initial values. The vortices cannot be started on the body because the time for a given vortex to leave the body is governed by a

logarithmic singularity. Two physical conditions were investigated for obtaining initial conditions to the equations of motion of the vortices. Firstly, the vortex motion in the immediate vicinity of the feeding points was examined by expanding the equations in Taylor series in terms of the vortex displacement from the feeding points. The expansion yielded independent relations for the motion of the two vortices with no connection between the time scales of the two motions. It also yielded the trajectories along which the vortices move in the near vicinity of the feeding points. Secondly, the behavior of the vortices far from the body was examined to determine if the time scales of the vortices could be connected using some property of their asymptotic behavior.

In order to integrate equations (5) the angle arguments of ζ_{o_1} and ζ_{o_2} must first be selected. Data on separation line location for the planar motion case at moderate angles of attack indicate the separation lines on the two flanks of the body to be symmetrical about a vertical plane through the body axis. For the lunar coning case where no data are available as a guide, the most reasonable first approximation is to assume that the separation lines are located symmetrically with respect to a plane through the body axis containing the vector sum of the $V\alpha$ and $\omega V\alpha(t_{cg} - t)$ crossflow velocities. Since the magnitude of the $\omega V\alpha(t_{cg} - t)$ component varies with time (or distance along the body) and its direction changes at t_{cg}, the plane containing the vector sum of the crossflow velocities will rotate in the x,y system with increasing time.

Calculation of Forces and Moments

The method of approach to the prediction of the force distribution on the body makes use of the Bernoulli equation to obtain the pressure distribution on the body, which is then integrated to obtain the force. In the non-rotating y',z' coordinate system, the force per unit length can be expressed as

$$\frac{dF'}{dx} = \frac{dY'}{dx} + i\,\frac{dZ'}{dx} = -e^{-i\omega t}\,\rho \int_c \frac{p}{\rho}\,d\zeta \qquad (6)$$

where the contour c is the periphery of the circle representing the

body, and the body nose is considered to pierce the plane fixed in the fluid (at $t = 0$) with the imaginary axes of the fixed (ζ') and rotating (ζ) coordinate systems aligned.

While the calculation of vortex motion can be accomplished in the rotating, ζ, coordinate system, some care must be exercised in distinguishing between the two axis systems in carrying out the force computation. It was noted previously that relative to the rotating, ζ, system, the flow over the body has an irrotational and a rotational part. In the ζ' system, the flow is completely irrotational and has the characteristic that all fluid velocities are zero at an infinite distance from the body. A velocity potential $\phi'(\zeta',t)$ exists, which is the real part of $W'(\zeta',t)$, given as follows

$$W'(\zeta',t) = V\alpha\left[i - \omega(t_{cg} - t)\right]\frac{a^2}{\left[\zeta' e^{i\omega t} - iV\alpha(t_{cg} - t)\right]}$$

$$+ a\dot{a}\ln\left[\zeta' e^{i\omega t} - iV\alpha(t_{cg} - t)\right]$$

$$- i\frac{\Gamma_1}{2\pi}\ln\left[\frac{e^{i\omega t}\left(\zeta' - \zeta'_{v_1}\right)}{\zeta' e^{i\omega t} - iV\alpha(t_{cg} - t) - \dfrac{a^2}{\overline{\zeta}'_{v_1} e^{-i\omega t} + iV\alpha(t_{cg} - t)}}\right]$$

$$- i\frac{\Gamma_2}{2\pi}\ln\left[\frac{e^{i\omega t}\left(\zeta' - \zeta'_{v_2}\right)}{\zeta' e^{i\omega t} - iV\alpha(t_{cg} - t) - \dfrac{a^2}{\overline{\zeta}'_{v_2} e^{-i\omega t} + iV\alpha(t_{cg} - t)}}\right] \tag{7}$$

The Bernoulli equation for unsteady flow in the ζ' system is given by paragraph 3.60 of reference 6 as

$$\frac{p}{\rho} = -\frac{\partial\phi'(\zeta',t)}{\partial t} - \frac{1}{2}\left(v'^2 + w'^2\right) + C(t) \tag{8}$$

where the constant C is uniform throughout the flow at a given instant of time. The procedure is to obtain the proper forms of the first two

terms on the right-hand side of equation (8) using the real part of equation (7) for $\phi'(\zeta',t)$ and the derivative of equation (7), $dW'(\zeta',t)/d\zeta'$ for $v' - iw'$. The contour integration indicated in equation (6) is then performed. With respect to the integration, it is noted in reference 7 for the case of free vortices external to a body that the contour can be enlarged from the body periphery to a contour with infinite radius, on the basis that inclusion of the external free vortices within the contour will not change the force computed on the body, since the external vortices are force-free. The advantage in so doing is that certain terms in the integrand go to zero in the integration. In the present case, the contour c may also be enlarged, since the condition of zero net force on the vortex plus its feeding sheet has been imposed. It is evident that when this procedure is carried out, the $v'^2 + w'^2$ terms in equation (8) go to zero for large ζ' and do not contribute to the integral. Also, since a contour integration is performed, the constant C in equation (8), which is constant everywhere on the contour, will not contribute. Thus the only term that does contribute in equation (6) is the time derivative of the velocity potential. In the integration it is convenient to use the relation

$$\frac{\partial \phi'(\zeta',t)}{\partial t} = \frac{\partial W'(\zeta',t)}{\partial t} - i \frac{\partial \psi'(\zeta',t)}{\partial t} \tag{9}$$

where $\psi'(\zeta',t)$ is the stream function for the flow, and the following relation between the coordinates

$$\zeta' = \left[\zeta + iV\alpha(t_{cg} - t) \right] e^{-i\omega t} \tag{10}$$

is used to obtain the results in the ζ system coordinates.

The application of this approach to the problem results in an expression for the force per unit length given by the following result,

$$\frac{dF'}{dx} = e^{-i\omega t}\left\{2\pi\rho a\dot{a}V\alpha\left[i - \omega(t_{cg} - t)\right]\right.$$
$$+ \pi a^2\rho\omega V\alpha\left[2 + i\omega(t_{cg} - t)\right]$$
$$+ \rho\omega\left[\Gamma_1\left(\zeta_{v_1} - \frac{a^2}{\bar{\zeta}_{v_1}}\right) + \Gamma_2\left(\zeta_{v_2} - \frac{a^2}{\bar{\zeta}_{v_2}}\right)\right]$$
$$+ \frac{\partial}{\partial t}\left[i\rho\Gamma_1\zeta_{v_1}\left(1 - \frac{a^2}{r_{v_1}^2}\right)\right]$$
$$\left. + \frac{\partial}{\partial t}\left[i\rho\Gamma_2\zeta_{v_2}\left(1 - \frac{a^2}{r_{v_2}^2}\right)\right]\right\} \qquad (11)$$

where

$$r_{v_j} = \left[\zeta_{v_j}\bar{\zeta}_{v_j}\right]^{1/2}$$

The first two terms represent forces that are derived from the attached flow around the body due to the body radius' changing with axial distance and the cross-coupling between the rotational and angle of attack motions. The next term arises from the motion of the vortices in the rotational flow around the body. The last two terms represent the time rate of change of impulse of each external vortex and its image, and are identical to the terms that occur for the planar motion case.

COMPUTER PROGRAM FOR VORTEX MOTION AND FORCES ON BODY

The differential equations (eq. (5)) which must be solved for the vortex motion are a set of first-order ordinary differential equations, linear in the derivatives. They can be written in the form

$$\frac{dy_1}{dt} = f_1(\zeta_1, \zeta_2, t)$$

$$\frac{dz_1}{dt} = f_2(\zeta_1, \zeta_2, t)$$

$$\frac{dy_2}{dt} = f_3(\zeta_1, \zeta_2, t)$$

$$\frac{dz_2}{dt} = f_4(\zeta_1, \zeta_2, t)$$

where

$$\zeta_1 = y_1 + iz_1$$

$$\zeta_2 = y_2 + iz_2$$

and f_1, f_2, f_3, and f_4 are real-valued functions. The expression for the complex force on the body (eq. (11)) is of this same form. The moments about the center of gravity of the body are obtained by integrating the following equations

$$\frac{dM}{dx} = V(t_{cg} - t)\frac{dZ}{dx}$$

$$\frac{dN}{dx} = V(t_{cg} - t)\frac{dY}{dx}$$

where the convention has been used that the pitching moment, M, is positive when produced by an upward force ahead of the center of gravity and the side moment, N, is positive when it corresponds to rotation of the nose to the right.

Integration of equations (5) is accomplished using a fourth-order Adams-Moulton predictor-corrector method (ref. 8) with starting values determined using a Runge-Kutta integration scheme. Initial values of ζ_1, ζ_2, and t are provided as input to the computer program. The initial values of the integrated forces and moments are defined to be zero.

The computer program written to integrate the equations consists of a main program and six subroutines. The main program reads the input data and controls the flow of the calculations. The various subroutines compute the derivatives and the vortex strengths, perform the integration, compute the coordinates of the body surface and separation points, and print out the information of interest.

The starting conditions for the vortex positions are input in either of two ways, as determined by the value of an index, NSTART. If NSTART = 0, the data to be input are the quantities ϵ_1 and ϵ_2 shown in figure 3. The initial vortex positions are subsequently calculated as

$$\zeta_{v_{1_i}} = \zeta_{o_1} + a\epsilon_1 \exp\left[i\left(\theta_{o_1} + \frac{\pi}{3} + \gamma_1\right)\right]$$

and

$$\zeta_{v_{2_i}} = \zeta_{o_2} + a\epsilon_2 \exp\left[i\left(\theta_{o_2} - \frac{\pi}{3} + \gamma_2\right)\right]$$

where ζ_{o_1} and ζ_{o_2} are the initial values of the locations of the separation points, and γ_1 and γ_2 are given by equation (A-13). If NSTART = 1 the data to be input are the coordinates y_{v_1}, z_{v_1}, y_{v_2} and z_{v_2} of the vortex positions. The initial coordinates of the separation points are computed as

$$\zeta_{o_1} = ae^{i(\theta_c - \theta_{s_1})} = ae^{i\theta_{o_1}}$$

$$\zeta_{o_2} = ae^{i(\theta_c + \theta_{s_2})} = ae^{i\theta_{o_2}}$$

where θ_{s_1} and θ_{s_2} are input and θ_c is the angle of the direction defined by the crossflow velocities $V\alpha$ and $\omega V\alpha(t_{cg} - t)$

$$\theta_c = \tan^{-1}\left[-\frac{V\alpha}{\omega V\alpha(t_{cg} - t)}\right]$$

INITIAL CONDITION ANALYSIS

Bryson (ref. 5) showed for his potential flow model of vortex shedding from a body in steady motion at an angle of attack that the vortex feeding points are unstable saddle points and, therefore, there is only one integral curve passing through each feeding point. Because of the unsymmetrical nature of the present problem, it was considered desirable to derive a linearized solution of the problem in the vicinity of the feeding points similar to that for the Bryson problem.

The analysis followed the same procedure as used by Bryson (Appendix B of ref. 5). First, the vortex positions were expressed as

$$\zeta_1 = \zeta_{o_1} + a\epsilon_1 e^{i\phi_1}$$

$$\zeta_2 = \zeta_{o_2} + a\epsilon_2 e^{i\phi_2} \tag{12}$$

where ζ_{o_1} and ζ_{o_2} are the complex coordinates of the feeding points, and ϵ_1 and $\epsilon_2 << 1$. The assumption of zero net vorticity previously discussed was used. The equations describing the vortex motion (eq. (5)) were evaluated to first order for small ϵ; and the induced velocity at a vortex, V_{v_j} was expanded in a Taylor series about the feeding point, ζ_{o_j}. The condition that the feeding points be stagnation points relative to the resultant crossflow was imposed. The details of the analysis are presented in Appendix A.

The assumption of small ϵ_j and the consequent neglect of terms of second order and higher order in ϵ_j resulted in decoupling the equations describing the motion of the two vortices. Thus, to first order in ϵ_j, two independent sets of equations were derived describing the paths along which the vortices move and the manner in which they move along their respective paths. The feeding points were shown to be unstable saddle points with a single integral curve passing through each, inclined at an angle of 30^o to the downstream tangent to the body at the feeding point. This result is identical to that of Bryson (ref. 5) for the case of planar motion. However, unlike the planar motion problem,

the a priori assumption of symmetry of vortex displacement is not justified in this case. The first-order analysis discussed here cannot yield any information about the relative displacements of the two vortices since, to first order, the vortices move independently of each other. The second-order analysis is quite extensive and is beyond the scope of the present effort. The independence of the linearized motion of the two vortices is illustrated in figure 4, where the variation of ϵ_1 and ϵ_2 with time is shown on a semi-logarithmic plot for two different values of ϵ_2/ϵ_1 with $\epsilon_1 = 10^{-6}$. The ratio of ϵ_2/ϵ_1 is constant at the initial value for both cases. The variation of ϵ_1 is the same in both cases while the variation of ϵ_2 is different by the ratio ϵ_2/ϵ_1. The logarithmic nature of the singularity at the feeding point ($\epsilon_j = 0$) is shown by the linearity of the variation of $\ln \epsilon_j$ with time.

Thus, although the linearized analysis is useful in determining the paths along which the two vortices move in the region near the separation points, it was not capable of providing a complete and unique set of initial conditions for calculation of the vortex motion and induced force distribution. Nor is it clear on a priori grounds that a second-order analysis will overcome the deficiency of the first-order analysis.

EFFECT OF INITIAL CONDITIONS ON ASYMPTOTIC VORTEX BEHAVIOR

An investigation was conducted to determine the sensitivity of the vortex behavior to the initial conditions. The investigation was carried out for cylindrical bodies as well as slender conical bodies.

Cylindrical Bodies

A systematic study of the effect of initial conditions on the downstream behavior of the vortices on a cylindrical body was conducted using the computer program written to solve equations (5). The initial vortex positions were defined as

$$\zeta_{v_j} = \zeta_{o_j} + a\epsilon_j e^{i\phi_j}$$

as in the near field analysis discussed above. The values of ϵ_j were provided as input to the computer program, along with the body radius and the locations of the feeding points. The angles, ϕ_j, were computed from the first-order analysis (eq. (A-10)). The initial location of the right-hand vortex was always specified as

$$\epsilon_1 = 0.05$$

while the initial value of ϵ_2 was varied.

Non-coning case.- The first step in the study of the downstream behavior was to examine the case of planar motion ($\omega = 0$) both with symmetrical initial values of ϵ and with small deviations from initial symmetry to gain insight into the effect of initial errors on the downstream behavior. Some results are shown in figure 5 for the case of $\alpha = 26^\circ$ and $\theta_s = 50^\circ$ with separation considered to originate at the nose at $t = 0$. Figure 5(a) shows the trajectories of the vortices for initial values of ϵ_2 of 0.049, 0.05, and 0.051. For the symmetrical case ($\epsilon_{2_i} = 0.05$), Bryson (ref. 5) shows that the vortices pass outside of and then curve in towards specific points on the Föppl curve determined by requiring that the velocity at the vortex and at the separation point be zero simultaneously. The vortices actually reach the points on the Föppl curve at $t = \infty$, since the induced velocity there is zero. Figure 5(a) illustrates this behavior for $\epsilon_{2_i} = 0.05$. For $\epsilon_{2_i} = 0.049$, the left-hand vortex lags behind the right-hand vortex and the Föppl point is not reached. For $\epsilon_{2_i} = 0.051$, the opposite effect occurs; the right-hand vortex lags behind the left.

The possibility exists with a numerical integration solution and a computer that round-off errors can introduce a source of asymmetry even in the case of symmetrical initial conditions. These errors can accumulate so that the asymmetry increases as the integration proceeds and can cause the solution to diverge markedly from the symmetrical case. The error limits of the Adams integration scheme used in the computer program described previously were established so that symmetry was maintained until the vortices reached the immediate vicinity of the Föppl line, the locus of vortex positions at which there is zero

induced velocity, V_v. The results of a computation with a sufficiently small error limit are shown as the solid curves in figure 5. The results of figure 5(b) indicate that the solution does not begin to diverge from the symmetrical case until a point some 55 radii from the nose is reached, at which point each vortex is near its Föppl point.

It is characteristic of the planar motion solution that the vortex strength will increase to a point about 30 radii downstream of the nose, at which point the vortex begins to curve towards the Föppl point and the vortex strength begins to decrease; that is, $\dot{\Gamma}$ becomes negative. At this point, the solution becomes physically unrealistic since the occurrence of negative $\dot{\Gamma}$ implies that vorticity is being fed back into the body boundary layer rather than being shed from the boundary layer.

In figure 5(b) is shown the variation of ϵ_1 and ϵ_2 with distance along the body for the three cases discussed above. In the symmetrical case, $\epsilon_1 = \epsilon_2$ until the divergence due to numerical errors occurs sometime after the Föppl point is reached, about 55 radii from the nose. In the asymmetrical cases either ϵ_1 or ϵ_2 exhibits a peak value at a station about 20 radii from the nose dependent upon whether ϵ_1 or ϵ_2 was larger initially.

In figure 5(c) are shown the variations of $\dot{\epsilon}$ for the two vortices. In the symmetrical case, $\dot{\epsilon}_1 = \dot{\epsilon}_2$ until the divergence due to numerical errors occurs. The value of $\dot{\epsilon}$ first rises to a maximum, then decreases and becomes negative as the vortices reach the vicinity of the Föppl point. The value of $\dot{\epsilon}$ then returns to zero as the Föppl point is approached. At this point the second derivative, $\ddot{\epsilon}$, also approaches zero. The same characteristic shape of the curve of $\dot{\epsilon}$ versus x is produced for the asymmetric cases. However, the condition $\dot{\epsilon}_1 = \dot{\epsilon}_2 = 0$ is never reached. Note, however, that when the initial value of ϵ_2 is lower than that for the symmetrical solution which reaches the Föppl point, then $\dot{\epsilon}_2$ becomes negative, but $\dot{\epsilon}_1$ does not. Conversely, when the initial value of ϵ_2 is larger than that for the symmetrical solution, $\dot{\epsilon}_1$ becomes negative, but $\dot{\epsilon}_2$ does not. More significantly, when ϵ_2 is initially smaller than the value for the symmetrical solution, the value of $\dot{\epsilon}_2$ is consistently smaller than $\dot{\epsilon}_1$ in the far field and conversely for initial values of ϵ_2 larger than required for the symmetrical solution.

Coning case.- One would expect to find with coning motion a downstream behavior of the vortices similar to that of the planar motion case, at least for small coning rates. This result is illustrated in figures 6, 7, and 8 for the case of $\omega \ell_{cg}/V = 0.12$ and $\epsilon_{1_i} = 0.05$. With $\epsilon_{2_i} = 0.05$ (fig. 6), the trajectory, the variations of ϵ_1 and ϵ_2 and of $\dot{\epsilon}_1$ and $\dot{\epsilon}_2$ are similar to the behavior noted above for the non-coning case where ϵ_{2_i} was less than ϵ_{1_i}. With $\epsilon_{2_i} = 0.054$ (fig. 7), the behavior of the vortex motion parameters is similar to the behavior for the non-coning case where ϵ_{2_i} was greater than ϵ_{1_i}. It is of interest to note that the small change in ϵ_{2_i} for the coning case results in a completely different downstream behavior as shown by comparison of figures 6(a) and 7(a).

The intermediate case with $\epsilon_{2_i} = 0.05320325$ is shown in figure 8. The behavior shown here is qualitatively similar to that shown for the non-coning case with symmetrical initial conditions, as shown in figure 5. Figure 8 indicates that the two vortices move away from their feeding points at similar rates. The vortices first accelerate, then slow and finally approach positions that are essentially stationary with respect to the resultant crossflow velocity vector. Furthermore, in the coning case, $\dot{\Gamma}$ becomes negative for both vortices at approximately 30 radii downstream as in the planar motion case, whereas $\dot{\Gamma}$ does not become negative for either vortex in the other two coning cases mentioned above. Thus, the downstream behavior of the vortices with coning motion is qualitatively the same as that for the planar motion case where symmetry exists, at least for moderate coning rates.

The principal vortex-induced force distribution is in the z direction. The side force distribution is an order of magnitude lower and is quite sensitive to the differences in vortex positions and strengths caused by small differences in initial conditions. This result is illustrated in figure 9, which shows the axial variation of the side force distribution corresponding to the three values of ϵ_{2_i} noted above. A value of $\epsilon_{2_i} = 0.05$ produces a large side force to leeward, whereas the other two values of ϵ_{2_i} produce small side

forces to windward. These results indicate the importance of obtaining a reliable method for determining initial conditions.

Conical Bodies

For the case of a slender cone at angle of attack with flow separation and vortex formation, Bryson (ref. 5) derived the vortex motion and forces on the assumption that the flow field is conical. Thus, solutions in the crossflow planes are similar and are scaled according to distance from the cone vertex. The present formulation of the problem does not employ such an assumption. Consequently, a number of calculations were made with conical bodies to check the Bryson results for the planar motion case and to determine the nature of the present solution for the coning case.

The behaviors of the vortices shed from a slender cone for both planar and coning motion are shown in figure 10. The configuration is a 10° half-angle cone with the center of gravity at $\ell_{cg}/\ell_{o} = 0.61$ for the coning case. The cone angle of attack is 34°. In both cases, the separation lines were specified at angles, θ_{s}, 34° from the resultant crossflow vector. In the coning case, two sets of initial conditions on ϵ_{1} and ϵ_{2} were used. The value of ϵ_{1_i} was specified as 0.05 in both sets of initial conditions while ϵ_{2_i} was given the values 0.05 and 0.055. In the planar motion case the initial values were $\epsilon_{1_i} = \epsilon_{2_i} = 0.05$. In all cases the starting positions of the vortices were specified on lines inclined 30° to the downstream tangents to the body at the feeding points. The variation of ϵ_{1} and ϵ_{2} for planar motion ($\omega = 0$) is indicated in figure 10 by a solid line, while the broken lines represent the variation for $\omega\ell_{cg}/V = 0.042$. The vortices in all cases were started at $x/\ell_{o} = 0.00191$. For the $\omega = 0$ case, the solution immediately converges to a value of $\epsilon = 0.3976$ with the vortices on lines 36.86° from the downstream tangents to the body at the feeding points.

In the coning case, the asymptotic solution is very sensitive to the initial conditions just as it is for the cylindrical body. For equal initial values of ϵ_{1} and ϵ_{2}, the solution converges very rapidly in the same manner as the planar motion case, but the asymptotic solution is one in which ϵ_{1} increases approximately linearly with

time and ϵ_2 decreases. For $\epsilon_2 = 0.055$, the downstream solution is characterized by even greater asymmetry.

Of the two sets of results for coning motion shown in figure 10, the set using symmetric initial conditions appears the most plausible in accordance with the following reasoning. In the planar motion case where the initial conditions and the locations of the separation lines are clearly symmetrical, a conical solution is obtained, which implies that the vortices originate on the axis of the cone at its apex. For the coning motion case (where the separation lines are also assumed to be symmetrical about the plane of the resultant velocity vector), the vortices should also originate on the cone axis at the apex. At the apex, the rotational flow field, which is the principal source of asymmetrical growth and motion of the vortices, is zero. Thus, one would expect the initial vortex motion and growth at the cone apex to resemble that for the planar motion case, and the motion just downstream of the apex should not be appreciably different from the planar motion case.

The results for the vortex strengths are shown in figure 11. In the planar motion case, the vortex strengths are equal and increase linearly with time, or distance along the body. In the coning case, the strengths still increase linearly with time, but at different rates.

COMPARISONS WITH DATA

Slender Cones

Unpublished data on a 10° half-angle cone were obtained from the Ames Research Center, NASA. The cone was mounted on a bent sting such that the sting could be rotated to produce the coning motion and the cone could be spun relative to the sting. The angle of attack could be varied using interchangeable stings. A six-component force balance system measured aerodynamic forces in body coordinates and moments about the center of gravity. Photographs were taken of the vortex positions at various axial stations using the vapor screen technique and a camera mounted on the rotating sting. The cone was mounted with its center of gravity at the 61-percent length station. Tests were

conducted in the Ames Research Center 6- by 6-Foot Wind Tunnel at the conditions as described earlier in this report.

Comparisons between the vortex positions deduced from vapor screen photographs and calculated positions for an angle of attack of 30°, a value of $\omega \ell_{cg}/V$ of 0.042, and a Mach number of 2.0 are shown in figure 12. The agreement is reasonably good. The feeding points for the theoretical calculation were chosen to be at angles, θ_s, symmetrically displaced 34° from the resultant crossflow vector. The value of 34° is the same as that used by Bryson (ref. 5) based on cone separation data. The initial vortex displacements were symmetrical with $\epsilon_1 = \epsilon_2 = 0.05$ in accordance with the reasoning of the previous section.

In comparing the forces and moments on the cone, it is useful to consider the forces due to both the attached and the separated flow around the body. In reference 4 it is shown that for small angles and angular rates (attached flow), the total side-moment coefficient can be expressed as

$$C_n = \frac{\omega \ell_o}{V} \alpha (C_{m_q} + C_{m_{\dot{\alpha}}}) \tag{13}$$

Similarly, the side-force coefficient can be expressed as

$$C_y = \frac{\omega \ell_o}{V} \alpha (C_{Z_q} + C_{Z_{\dot{\alpha}}}) \tag{14}$$

Reference 9 indicates that slender-body theory considerably overpredicts the stability derivatives, C_{Z_q}, $C_{Z_{\dot{\alpha}}}$, C_{m_q}, $C_{m_{\dot{\alpha}}}$ for a cone at supersonic flight Mach numbers. Therefore, since the attached flow portion of the forces and moments in the present theory are based on slender-body theory, it is appropriate to examine only the nonlinear, or vortex-induced, forces and moments.

Figure 13 shows the comparison between theory and data for the variation of side-force coefficient, $C_y/(\omega \ell_o/V)$, with angle of attack. The theory is indicated by open symbols while the experiment is indicated by filled circles. Theoretical results for two values of the

separation line location, θ_s, are shown. The linear variation of $C_y/(\omega \ell_o/V)$ for small angles of attack is predicted very well by the results of reference 9 as shown in the figure. The predicted values at high angles of attack were obtained by adding to the linear variation for attached flow the predicted nonlinear contributions due to the vortices. In figure 14 the theoretical side moment on the cone is compared with the experimental data in the same manner as for the force coefficient above.

Figures 13 and 14 indicate that the predicted results are strongly influenced by the location of the vortex feeding points. For a given value of θ_s, the vortex-induced side force first appears at a larger angle of attack than the data indicate and increases at a faster rate than the data as the angle of attack is increased. The figures indicate that it may be possible to improve the prediction of the side force if θ_s is varied with angle of attack. This result is in qualitative agreement with the data of reference 10, where the angle of separation, θ_s, on inclined bodies in planar motion is shown to depend strongly on angle of attack. Also, it may be necessary to specify an axial variation of the separation line location different than the constant angular displacement from the resultant crossflow vector as used in the present theory. It is apparent that knowledge of the separation line location is an important factor in developing a predictive technique.

Ogive Cylinders

Some experimental measurements of side moments on a slender ogive-cylinder body are presented in reference 4. As in the cone experiments, vapor screen photographs were used to observe the vortices. The total side moment ahead of the center of gravity was measured. The configuration is a cylinder 2.5 inches in diameter with a fineness-ratio 3.4 tangent-ogive nose. The center of gravity was 2.5 feet from the nose of the body. The tests were run in the Ames Research Center 6- by 6-Foot Wind Tunnel with conditions as described earlier in this report.

Theoretical calculations of the vortex-induced forces on the ogive cylinder were made based on the assumption that the vortices started on the ogive nose of the body. Initial vortex positions were obtained

from calculations for a cone based on the conclusion reached previously that a unique set of initial conditions can be obtained for the solution for a cone. Essentially, the ogive-cylinder is considered to have a conical nose, and a cone solution like that discussed in the previous section is used to supply initial conditions for an ogive-cylinder calculation. The initial conditions were obtained as follows. First the station at which the tangent to the ogive surface made an angle of 10° with the body axis was found. The dimensions of a 10° half-angle cone tangent to the ogive at the same station were computed. Then the solution for the vortex motion over the cone was computed for the experimental conditions. The separation points were each assumed to be angles, θ_s, 50° from the resultant crossflow vector, which value corresponds to measured separation line locations on ogive-cylinders and cone-cylinders at angle of attack (ref. 10). The angle of 50° was chosen as the best estimate of an average value of the angular location of the separation line since the location actually varies along the body, whereas the computer program used here can only handle constant values of θ_s. The asymptotic solution for the vortex trajectories on the cone was then used to obtain the positions of the vortices on the ogive at the station at which the ogive was tangent to the 10° cone.

The results for the predicted vortex positions for an angle of attack of 26° and a coning rate ($\omega \ell_{cg}/V$) of 0.12 are compared with sketches made from unpublished vapor screen photographs for three axial stations in figure 15. While the "centers" of the areas of concentrated vorticity are difficult to determine, the predicted vortex positions tend to agree qualitatively with the photographic information. The theory predicts that the right-hand vortex is further away from the body than the left-hand vortex. The right-hand vortex has a greater strength than the left-hand vortex until a point about 10 radii from the nose, beyond which the strength of the left-hand vortex becomes larger.

The side-moment coefficient on the portion of the body from the nose back to the center of gravity is attributable almost entirely to the vortex-induced side force distribution, since slender-body theory for the attached flow predicts a zero value of $C_{m_q} + C_{m_{\dot{\alpha}}}$ for this case. This conclusion is substantiated by the data presented in reference 4, which is reproduced as figure 16. The predicted side moment at 26° is

also shown in figure 16, and falls within the scatter in the data. Thus, use of the cone solution as a source of initial conditions appears to be a promising technique for obtaining a unique solution for sharp-nosed non-conical bodies.

It is of interest to examine the photographs of the vortex positions near the aft end of an ogive-cylinder mounted and tested at the Ames Research Center in the same manner as was indicated previously for the 10° half-angle cone. In these tests, photographs of the vortex positions were obtained up to 8 diameters aft of the center of gravity. Sketches of the areas of concentrated vorticity for $\alpha = 25^{\circ}$ and $\omega \ell_{cg}/V = 0.12$ are shown in figure 17. Near the aft end of the body, the photographs tend to indicate that the right-hand vortex is "torn" from the separation line and becomes free, much as occurs on long slender bodies in planar motion at high angles of attack. Theoretical solutions for the ogive-cylinder indicate that generally $\dot{\Gamma}$ for the right-hand vortex becomes small but not necessarily zero at some point along the body. An example of this behavior is shown in figure 18 where the variation of $\dot{\Gamma}$ along the body is shown for both vortices for the ogive-cylinder case discussed above. Other calculations showed that $\dot{\Gamma}$ can become negative for certain combinations of initial conditions, angle of attack, coning rate, and separation line locations. Such behavior suggests that the tearing of the feeding sheet of one vortex might occur at the point where $\dot{\Gamma}$ becomes negative, and a new bound vortex would be started at the separation point. No calculations were made along these lines, however.

CONCLUDING REMARKS

Based on experimental evidence of the existence of a steady asymmetric vortex system on a slender body in coning motion, a theoretical flow model for vortex shedding was developed using potential flow methods and slender-body theory. The model provides for the calculation of the strength and position of each of the two vortices representing the areas of concentrated vorticity and the resulting force distribution induced on the body. For cylindrical bodies, initial vortex locations very close to the body must be prescribed to start the computation. The results for vortex motion and forces were found to be quite

sensitive to the initial asymmetry. In order to investigate the nature of the initial condition problem, a linearized analysis of the vortex motion very close to the body was performed. Linearization was found to decouple the motion of the two vortices, so that the paths of the vortices could be obtained, but the relative positions of the two vortices along their paths could not. Upon specializing the body to a cone, it was found that the full nonlinear solution rapidly converged to a unique solution for symmetrical initial conditions, but that the solution was again quite sensitive to initial conditions. It was reasoned that for the cone, with separation starting at the nose, the most likely initial conditions for the coning case were the symmetric vortex displacements found for the planar motion case. The symmetric solution was then used as a source of initial conditions for an ogive cylinder by considering the ogive to have a conical tip.

On the basis of agreement with data for a cone and an ogive cylinder in lunar coning motion, the flow model developed herein is felt to describe reasonably accurately the nature of the vortex-like separated flow over the body and the vortex-induced force distribution. The windward vortex is shown to be somewhat further distant from the body than the leeward vortex and to be somewhat stronger than the leeward vortex over the forward portion of the body. These differences are shown to produce a side force to leeward and a stabilizing side moment in correspondence with the measured results.

The dependency of the theoretical solution on assumptions regarding the separation line location should be noted. For the lunar motion case, the body is not spinning relative to the boundary layer, so that use of separation location data obtained for planar motion should be a reasonable assumption. On the basis of this assumption, one could probably devise some simple qualitative rules for the vortex strength and position behavior from the present analysis, which could be used in a fashion similar to the one shown in reference 4. However, the development of a truly predictive method requires a three-dimensional boundary layer solution that would predict the location of the separation lines over the length of the body. Such a method would then permit calculation of not only the lunar case but the case of coning motion with nonlunar spin rates, where the body is spinning relative to the boundary-layer flow and causing some shift in the location of separation.

Finally, the nature of the theoretical solution suggests some interesting possibilities for explaining other experimentally observed separation characteristics on slender bodies. Vapor screen photographs of an ogive cylinder in lunar coning motion tend to indicate that the sheet feeding the windward vortex eventually "tears," leaving that vortex "free" and forming a new vortex at the separation line. The theoretical results indicate that at some station aft along the body, the rate of change of strength of the windward vortex approaches zero or goes negative, which suggests that since vorticity is no longer being fed to the vortex from the separation line, the sheet should be cut. Further, an initial condition investigation for the planar motion case indicates that if the solution is perturbed asymmetrically, the asymmetry will grow in a fashion that resembles the coning motion solution. This result is in accordance with experimental observations of vortex flow over bodies at relatively high angles of attack, which tend to indicate the existence of a steady asymmetric vortex pattern, with sheets being torn and free vortices formed.

Nielsen Engineering & Research, Inc.
Palo Alto, Calif.
June 1969

APPENDIX A

DERIVATION OF MOTION OF VORTICES IN THE VICINITY OF FEEDING POINTS

Let the vortex positions be expressed as

$$\zeta_j = \zeta_{o_j} + a\epsilon^{i\phi_j} \tag{A-1}$$

where ζ_{o_j} is the complex coordinate of the feeding point of vortex j, as shown in the sketch below, and $\epsilon_j \ll 1$.

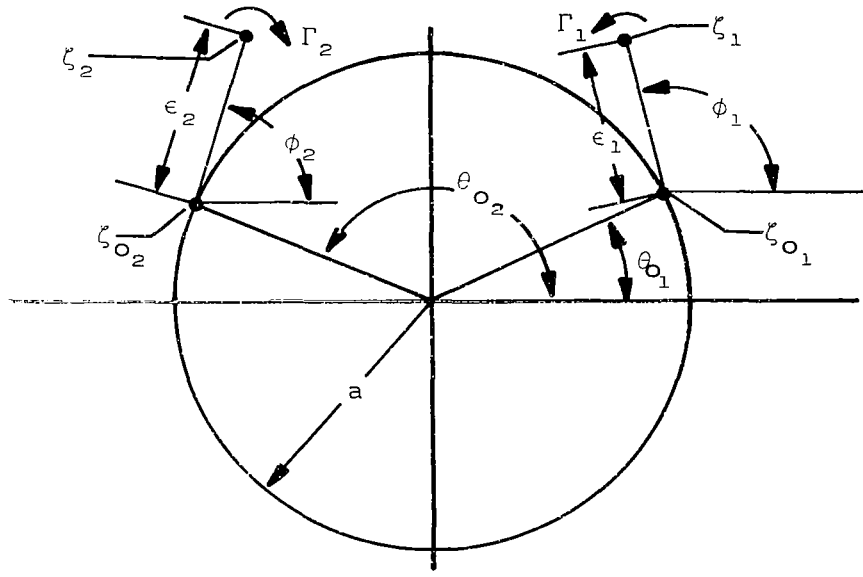

Assume

$$\Gamma_m = \Gamma_1 + \Gamma_2 \tag{A-2}$$

The expression for the vortex strengths resulting from equation (3) of the text becomes

$$\Gamma_j = \frac{1}{2}\epsilon_j V a \beta_j \sec(\phi_j - \theta_{o_j}) \qquad j = 1 \text{ or } 2 \tag{A-3}$$

where

$$\beta_j = \left[2\alpha \cos \theta_{o_j} + 2\omega\alpha(t_{cg} - t) \sin \theta_{o_j} + \frac{\omega}{V} a - \frac{\dot{\theta}_{o_j}}{V} a \right] e^{-i\theta_{o_j}}$$

or

$$\beta_j = R_j e^{-i\theta_{o_j}} \tag{A-4}$$

where R_j is a real-valued function, and time, t, is measured from the instant the nose of the body passes an arbitrary fixed plane in the fluid. Then the equations describing the vortex motion (eq.(5)) become

$$a\dot{\epsilon}_j e^{i\phi_j} = \frac{1}{2} V_{v_j} + \frac{1}{2} a\epsilon_j \left[\dot{\theta}_{o_j} \tan(\phi_j - \theta_{o_j}) - \frac{\dot{R}_j}{R_j} - 2 \frac{\dot{a}}{a} \right] e^{i\phi_j} - \frac{\dot{\zeta}_{o_j}}{2} \tag{A-5}$$

where terms containing $\epsilon_j \dot{\phi}_j$ have been considered to be of second order and neglected.

Now, ϕ_j is determined as follows. Expand the induced velocity at a vortex, V_{v_j}, in a power series in ϵ_j for fixed ϕ_j.

$$V_{v_j} = V_j^o(\phi_j) + \epsilon_j V_j^1(\phi_j) + \ldots \tag{A-6}$$

where $j = 1$ and 2, and

$$V_j^o(\phi_j) = e^{i\theta_{o_j}} \left\{ \left[2iV\alpha \cos \theta_{o_j} + 2i\omega V\alpha(t_{cg} - t) \sin \theta_{o_j} + i\omega a \right] \left[1 - \frac{1}{4} \sec^2(\phi_j - \theta_{o_j}) \right] + \dot{a} + i \frac{a}{4} \dot{\theta}_{o_j} e^{i\theta_{o_j}} \sec^2(\phi_j - \theta_{o_j}) \right\} \tag{A-7}$$

Now, when $\epsilon_j = 0$, $V_{v_j} = \dot{\zeta}_{o_j}$, so equation (A-6) requires

$$V_j^o(\phi_j) = \dot{a}e^{i\theta_{o_j}} + ia\dot{\theta}_{o_j}e^{i\theta_{o_j}} \tag{A-8}$$

Substituting equation (A-8) into (A-7) yields

$$1 - \frac{1}{4}\sec^2(\phi_j - \theta_{o_j}) = 0$$

whence

$$\phi_j - \theta_{o_j} = -(-1)^j \frac{\pi}{3} \tag{A-9}$$

Thus, both vortices leave their respective separation points along lines inclined 30° from the downstream tangents to the body at the positions of the separation points at the instant of separation. This is exactly the same condition that results for the case of symmetric vortex shedding from a body in steady motion at an angle of attack (Bryson's result).

The investigation of the stability of the feeding points and the early motion of the vortices proceeds as follows. Express the angle, ϕ_j, as

$$\phi_j = \theta_{o_j} - (-1)^j \frac{\pi}{3} + \gamma_j \tag{A-10}$$

where $\gamma_j << 1$. Expand the velocity $V_j^o(\phi_j)$ in a Taylor series about $\gamma_j = 0$, and evaluate $V_j^1(\phi_j)$ at $\gamma_j = 0$.

Thus,

$$V_j^o = \left(\dot{a} + ia\dot{\theta}_{o_j}\right)e^{i\theta_{o_j}} + 2i\sqrt{3}(-1)^j VR_j e^{i\theta_{o_j}}\gamma_j \tag{A-11}$$

and

$$V_j^1 = -2iV\alpha\left[1 - i\omega(t_{cg} - t)\right]e^{i\left[2\theta_{o_j} + (-1)^j \frac{\pi}{3}\right]}$$

$$+ i\omega a e^{i\left[\theta_{o_j} - (-1)^j \frac{\pi}{3}\right]} - \dot{a}e^{i\left[\theta_{o_j} + (-1)^j \frac{\pi}{3}\right]}$$

$$- iVR_j\left[e^{i\left[\theta_{o_j} - (-1)^j \frac{\pi}{3}\right]} - 2e^{i\theta_{o_j}}\right] \qquad \text{(A-12)}$$

Substituting equations (A-11) and (A-12) into equation (A-6) and subsequently into equation (A-5) and then separating into real and imaginary parts, yields from the real part,

$$\gamma_j = \epsilon_j \frac{A}{B} + \ldots \qquad \text{(A-13)}$$

where

$$A = -2V\alpha\left\{\cos\left[\theta_{o_j} - (-1)^j \frac{\pi}{3}\right] + \omega(t_{cg} - t)\sin\left[\theta_{o_j} - (-1)^j \frac{\pi}{3}\right]\right\}$$

$$+ \frac{1}{2}(-1)^j\sqrt{3}\,\dot{a} - \omega a$$

and

$$B = (-1)^j\sqrt{3}\,VR_j$$

Then, from the imaginary part,

$$\dot{\epsilon}_j = \epsilon_j\left\{\frac{1}{2a}\left(V_{R_j}^1 \cos\phi_j + V_{I_j}^1 \sin\phi_j\right) - \frac{1}{2}(-1)^j\sqrt{3}\,\dot{\theta}_{o_j}\right.$$

$$\left. - \frac{1}{2}\frac{\dot{R}_j}{R_j} - \frac{\dot{a}}{a} - \frac{1}{4}\left[(-1)^j\sqrt{3}\,\frac{\dot{a}}{a} + \dot{\theta}_{o_j}\right]\frac{A}{B}\right\}$$

$$+ \frac{1}{2a}\left(V_{R_j}^o \cos\phi_j + V_{I_j}^o \sin\phi_j\right) - \frac{1}{4}\left[\frac{\dot{a}}{a} - (-1)^j\sqrt{3}\,\dot{\theta}_{o_j}\right] + \ldots$$

(A-14)

where $V^o_{R_j}$, $V^1_{R_j}$, $V^o_{I_j}$, $V^1_{I_j}$ are the real and imaginary parts of V^o_j and V^1_j. It can be shown from equation (A-14) that when $\epsilon_j = 0$, then $\dot{\epsilon}_j = 0$. Thus, each vortex feeding point is an unstable saddle point with a single integral curve passing through it, given by equations (A-10) and (A-13).

It is of interest to compare equation (A-13) with the results of Bryson for the case of $\omega = \dot{a} = 0$. Equation (A-13) becomes

$$\gamma_j = -\epsilon_j \frac{\cos\left(\theta_{o_j} - (-1)^j \frac{\pi}{3}\right)}{(-1)^j \sqrt{3} \cos \theta_{o_j}}$$

which, for $j = 1$, gives Bryson's result

$$\gamma = \epsilon \frac{\cos\left(\frac{\pi}{3} + \theta_o\right)}{\sqrt{3} \cos \theta_o}$$

REFERENCES

1. Allen, H. J. and Perkins, E. W.: A Study of Effects of Viscosity on Flow over Slender Inclined Bodies of Revolution. NACA Rep. 1048, 1951.

2. Mello, J. F.: Investigation of Normal Force Distribution and Wake Vortex Characteristics of Bodies of Revolution at Supersonic Speeds. Jour. of Aero. Sci., vol. 26, no. 3, Mar. 1959, pp. 155-168.

3. Perkins, E. W. and Jorgensen, L. H.: Comparison of Experimental and Theoretical Normal Force Distribution on an Ogive Cylinder Body at M = 1.98. NACA TN 3716, 1956.

4. Tobak, M., Schiff, L. B., and Peterson, V. L.: Aerodynamics of Bodies of Revolution in Nonplanar Motion. AIAA Jour., vol. 7, no. 1, Jan. 1969, pp. 75-82.

5. Bryson, A. E.: Symmetric Vortex Separation on Circular Cylinders and Cones. Jour. of Appl. Mech., Dec. 1959, pp. 643-648.

6. Milne-Thomson, L. M.: Theoretical Hydrodynamics. Fourth Ed., The MacMillan Co., New York, N. Y., 1960.

7. Sacks, A. H.: Vortex Interference on Slender Airplanes. NACA TN 3525, Nov. 1955.

8. Hildebrand, F. B.: Introduction to Numerical Analysis. McGraw-Hill Book Co., New York, N. Y., 1956, Chapter 6.

9. Tobak, M. and Wehrend, W. R.: Stability Derivatives of Cones at Supersonic Speeds. NACA TN 3788, Sept. 1956.

10. Spangler, S. B., Sacks, A. H., and Nielsen, J. N.: The Effect of Flow Separation from the Hull on the Stability of a High-Speed Submarine. Part I. Theory. Vidya Rep. No. 107, Aug. 15, 1963.

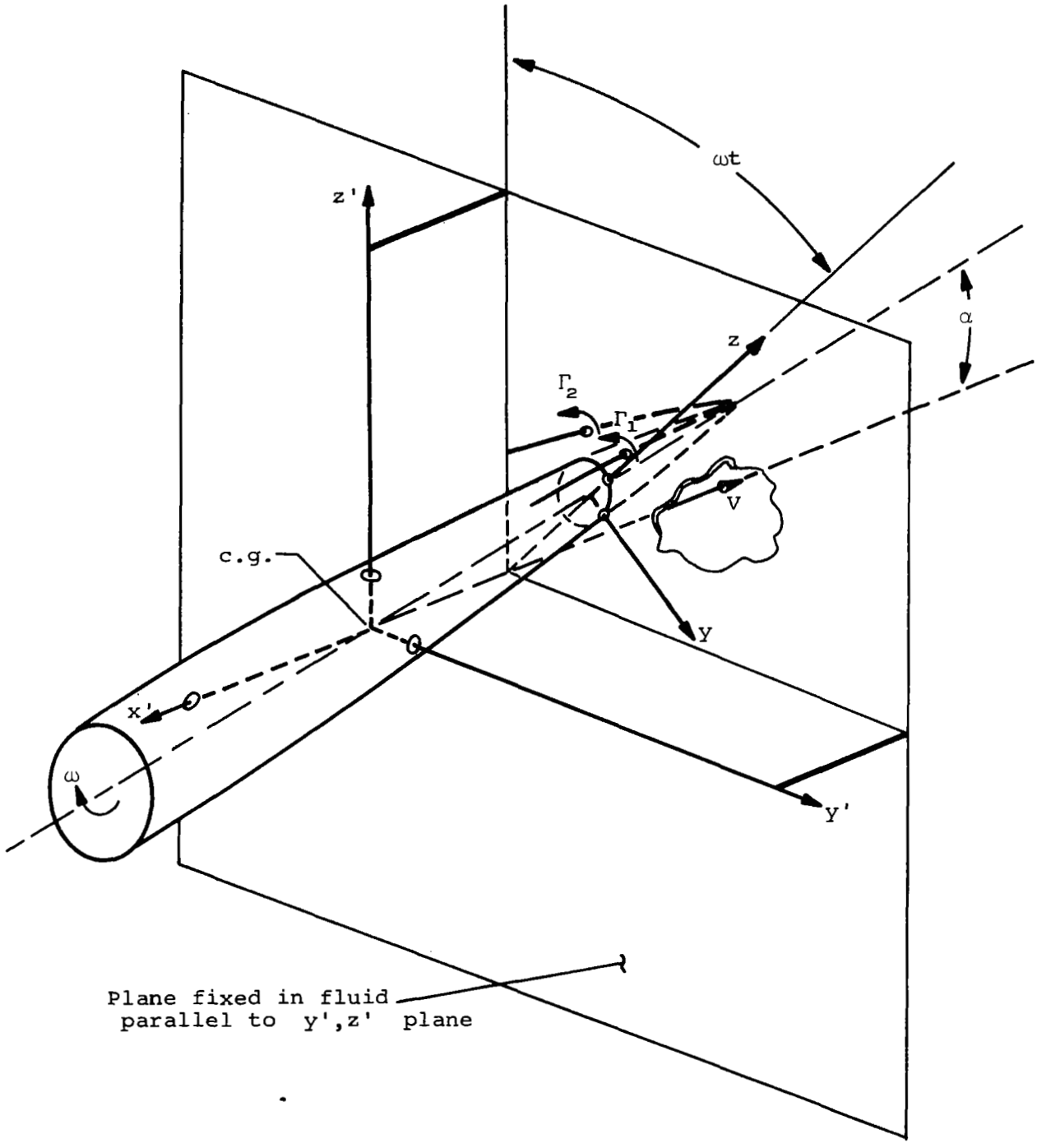

Figure 1.- Sketch of the motion of the body through the fluid.

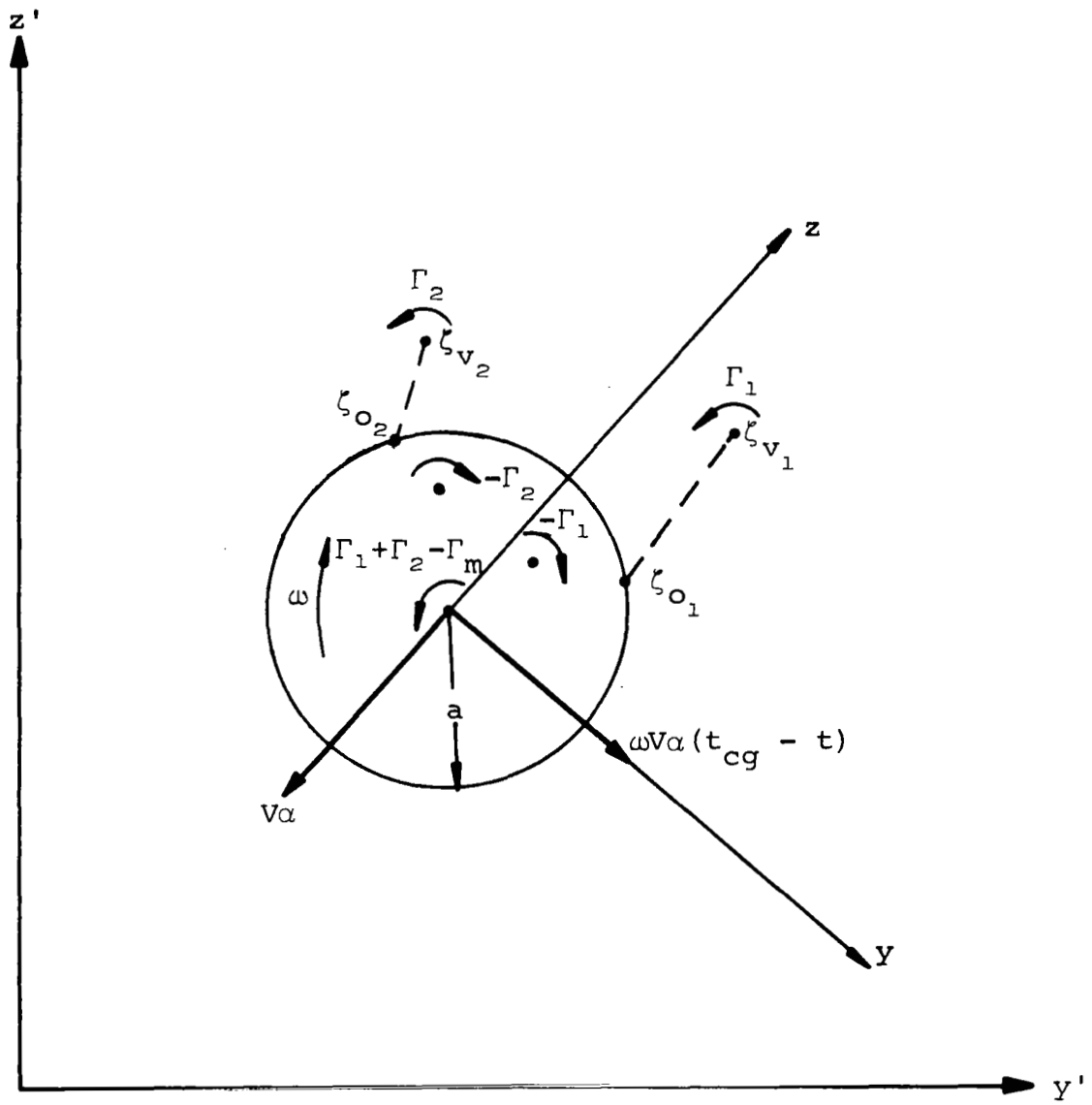

Figure 2.- Flow field in the plane fixed in the fluid.

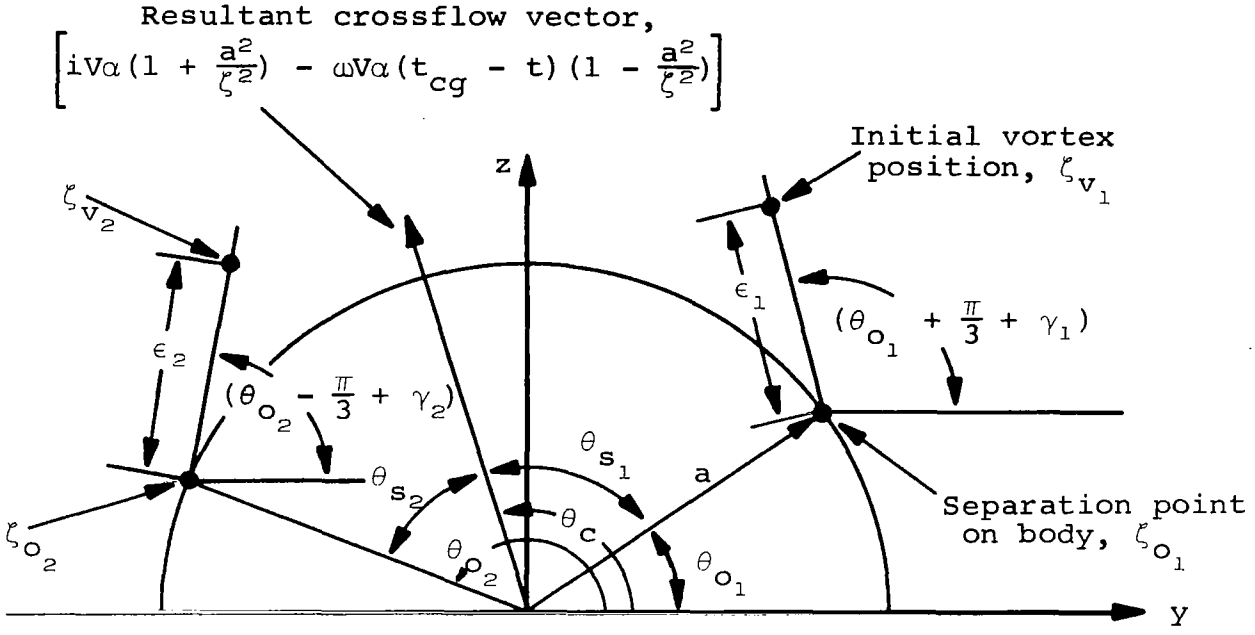

Figure 3.- Coordinates for computer program input data.

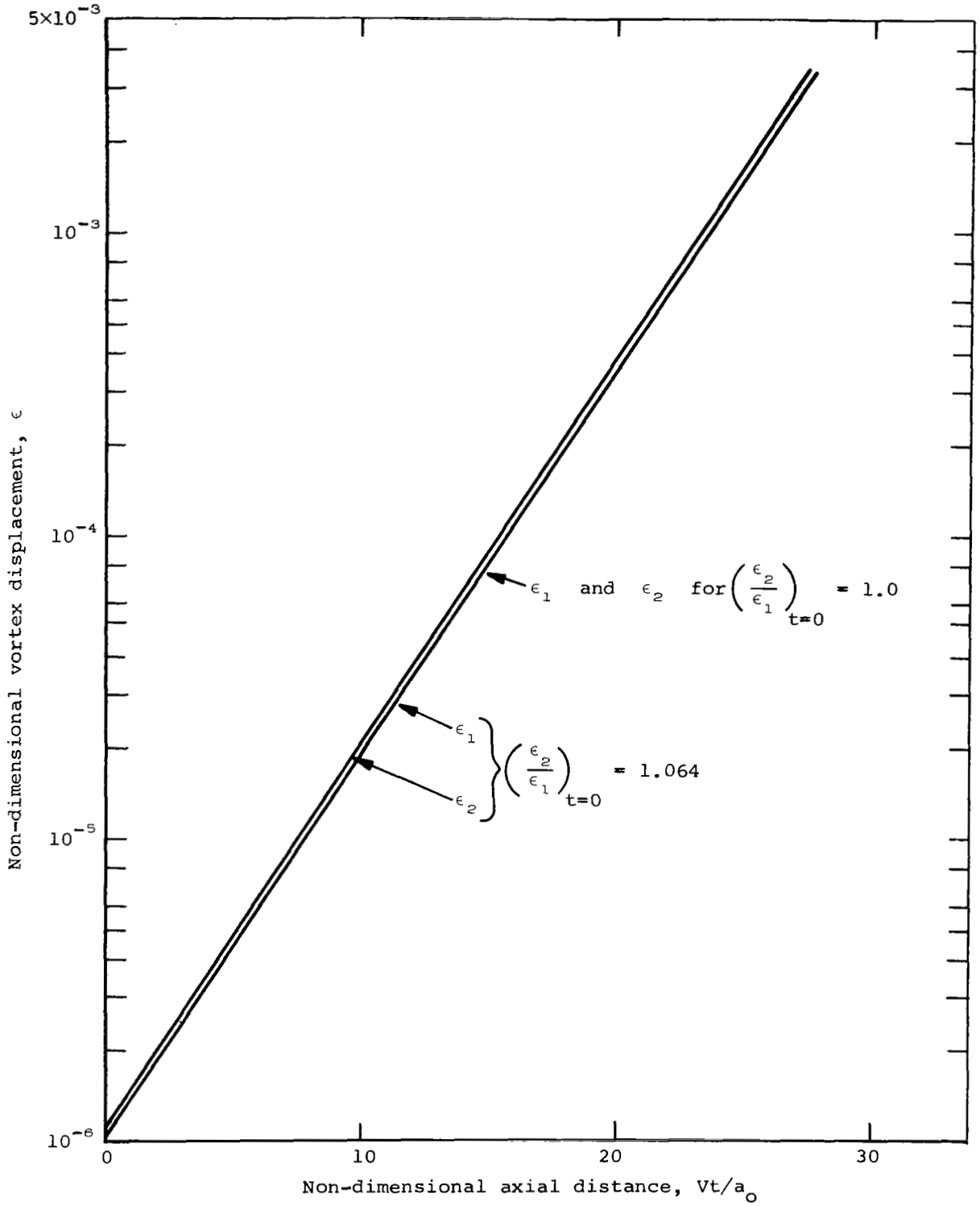

Figure 4.- Linearized solution for non-dimensional vortex displacement, $\alpha = 26^{o}$, $\omega \ell_{cg}/V = 0.24$.

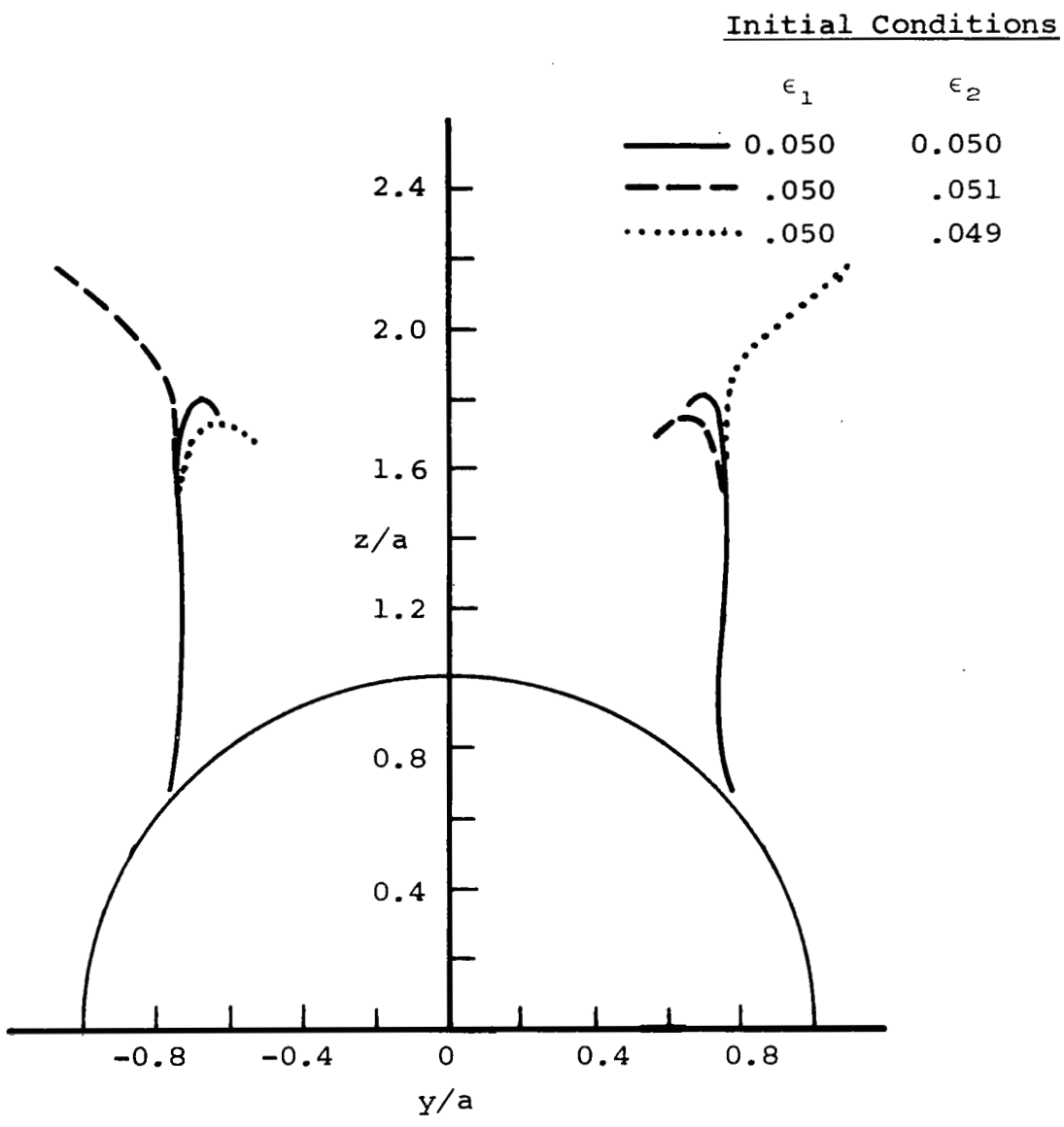

(a) Vortex trajectories.

Figure 5.- Vortex motion on a cylindrical body in planar motion for different initial conditions, $\alpha = 26^{o}$, $\omega \ell_{cg}/V = 0.0$.

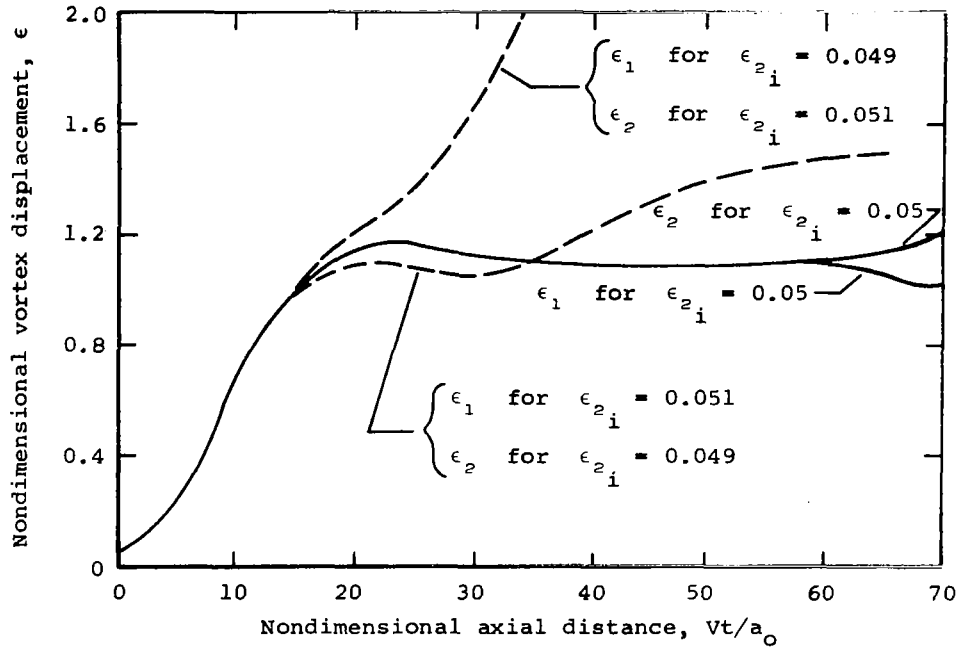

(b) Vortex displacement.

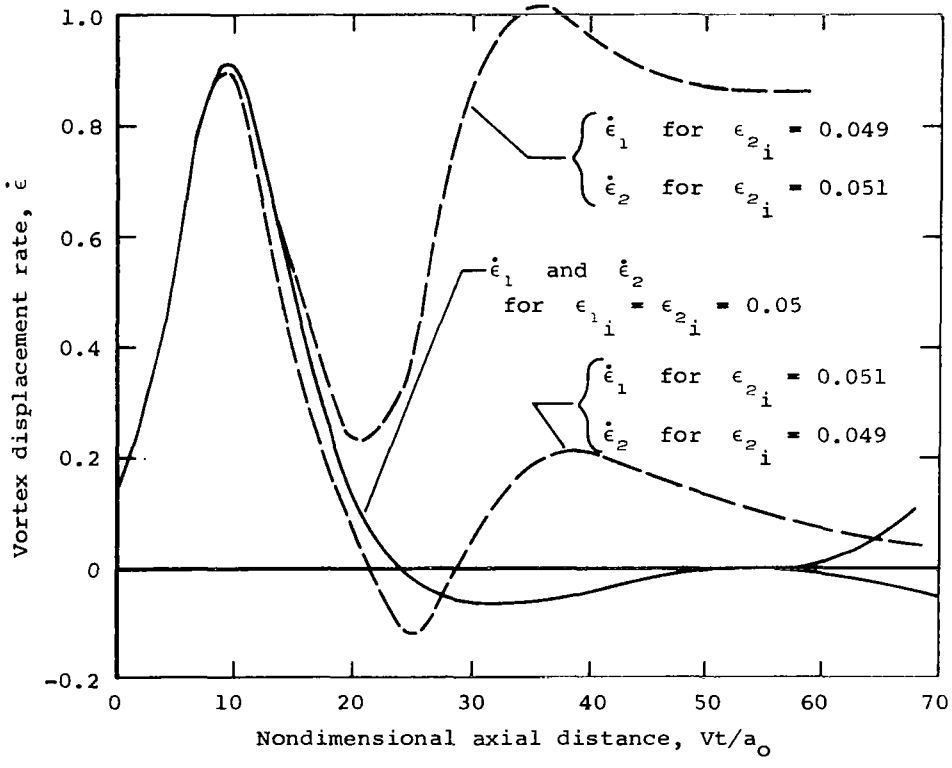

(c) Vortex displacement rate.

Figure 5.- Concluded.

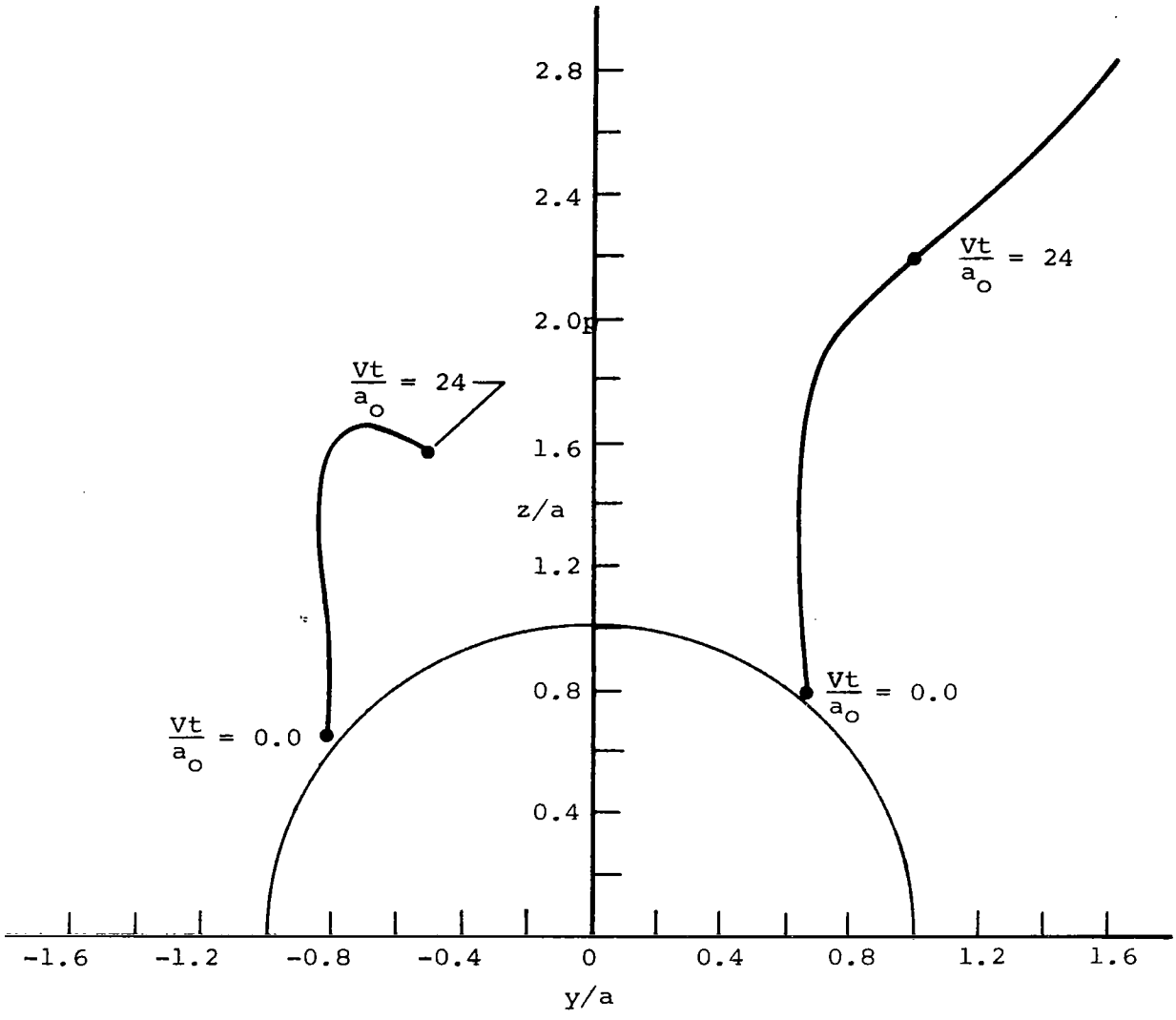

(a) Vortex trajectories.

Figure 6.- Vortex motion on a cylindrical body in coning motion for symmetrical initial conditions, $\epsilon_{1_i} = \epsilon_{2_i} = 0.05$, $\omega \ell_{cg}/V = 0.12$.

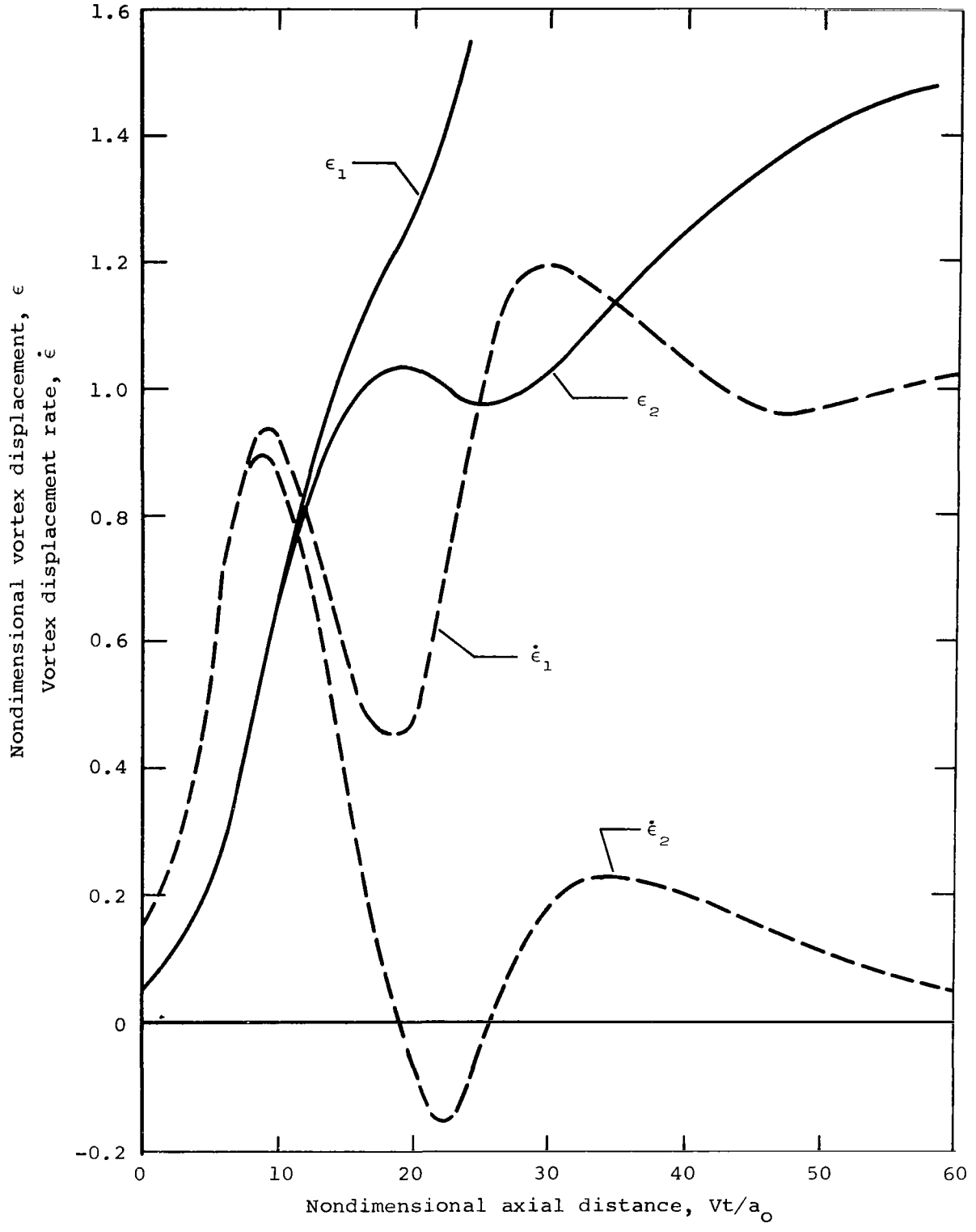

(b) Vortex displacement and displacement rate.

Figure 6.- Concluded.

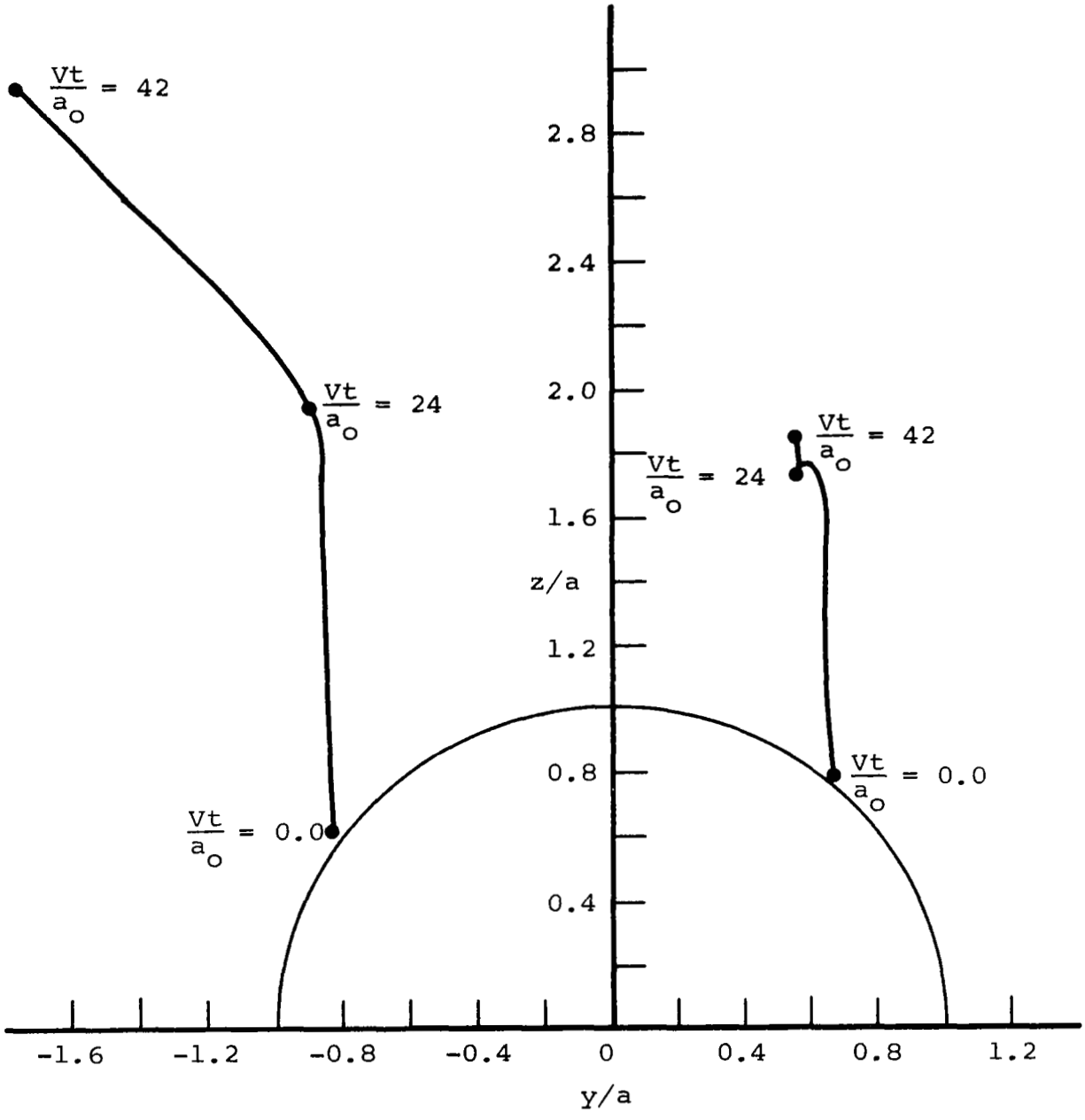

(a) Vortex trajectories.

Figure 7.- Vortex motion on a cylindrical body in coning motion for unsymmetrical initial displacements, $\epsilon_{1_i} = 0.05$, $\epsilon_{2_i} = 0.054$, $\alpha = 26^{\circ}$, $\omega \ell_{cg}/V = 0.12$.

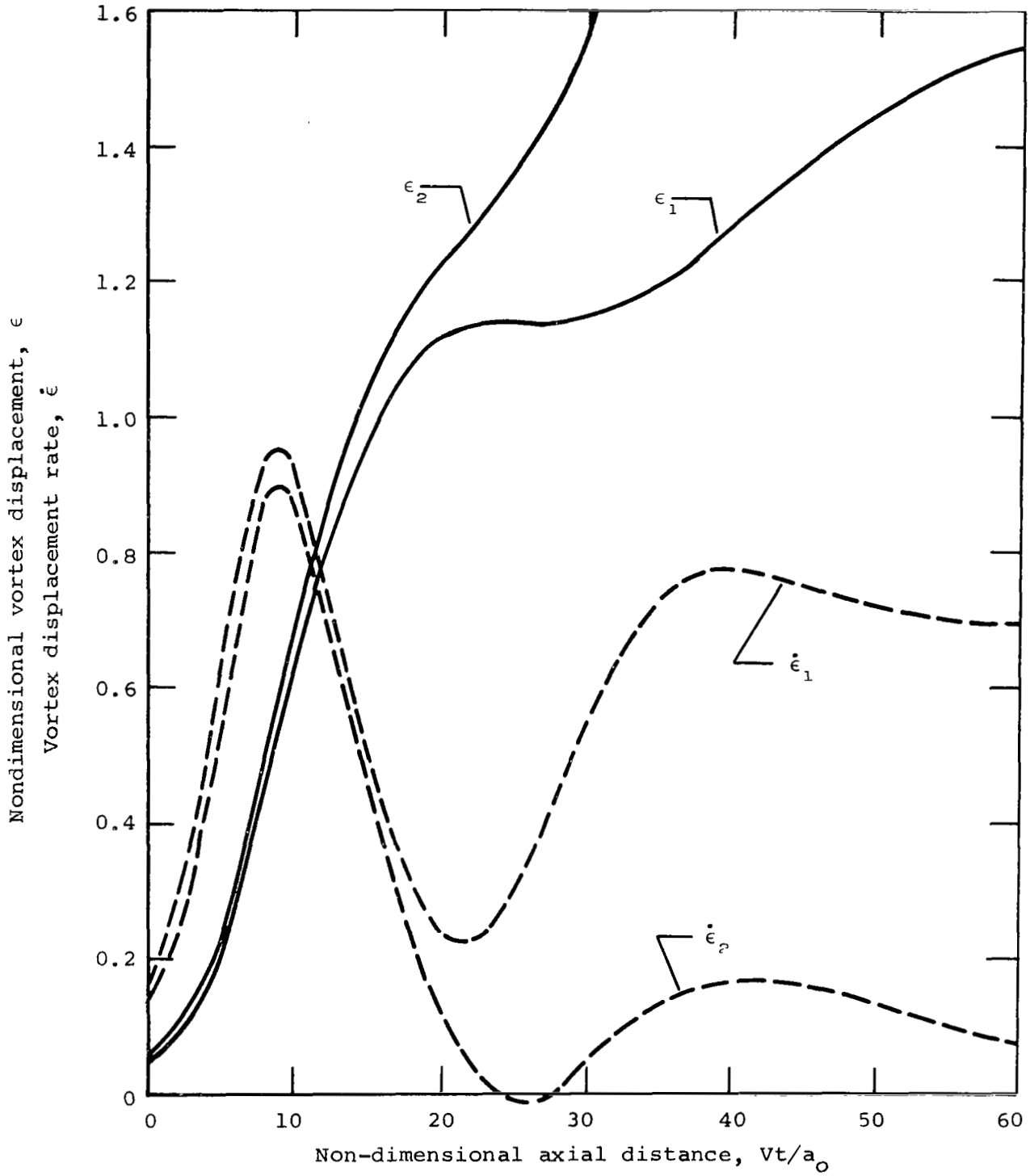

(b) Vortex displacement and displacement rate.

Figure 7.- Concluded.

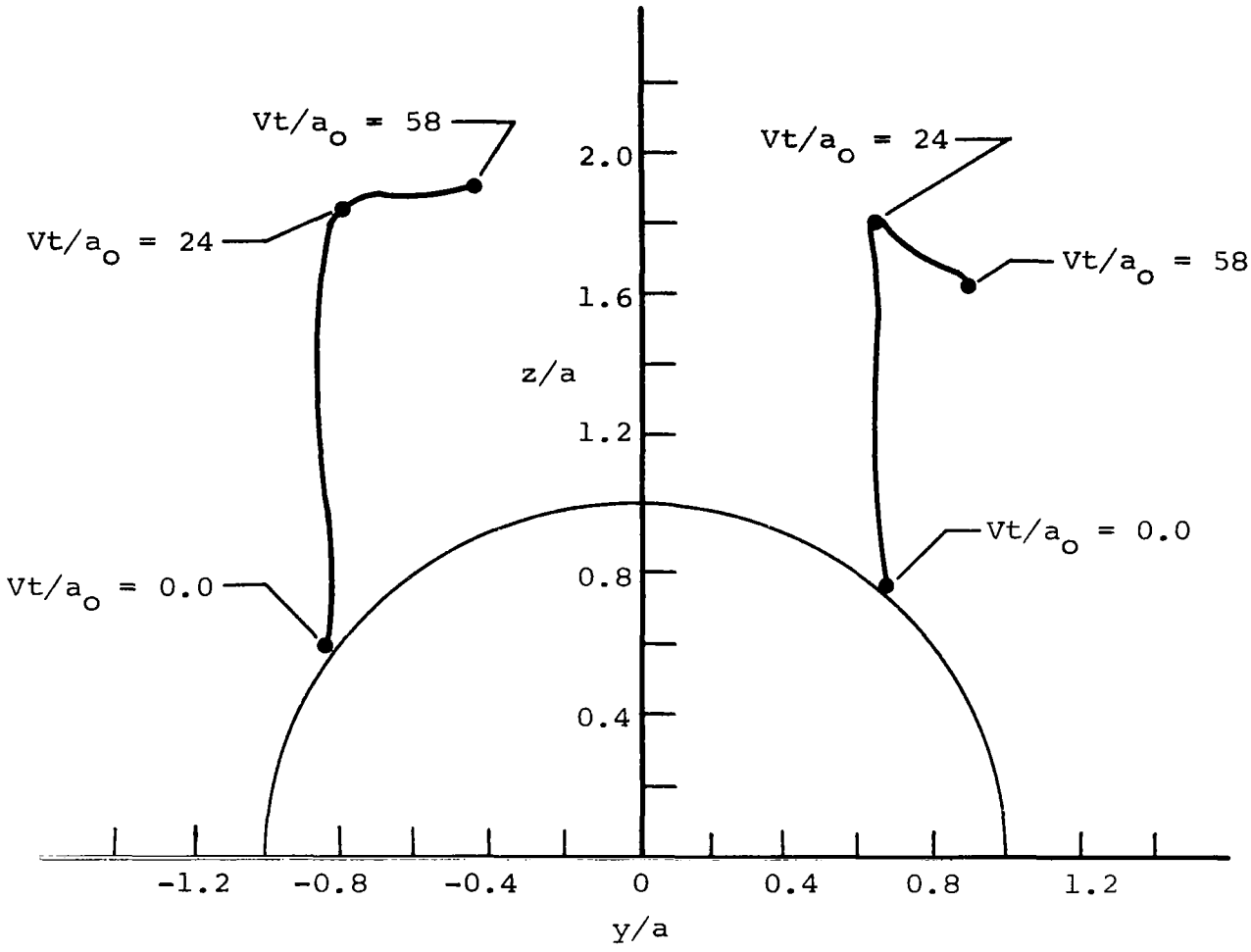

(a) Vortex trajectories.

Figure 8.- Vortex motion on a cylindrical body in coning motion for unsymmetrical initial displacements; $\epsilon_{1_i} = 0.05$, $\epsilon_{2_i} = 0.05320325$, $\omega \ell_{cg}/V = 0.12$, $\alpha = 26^{\circ}$.

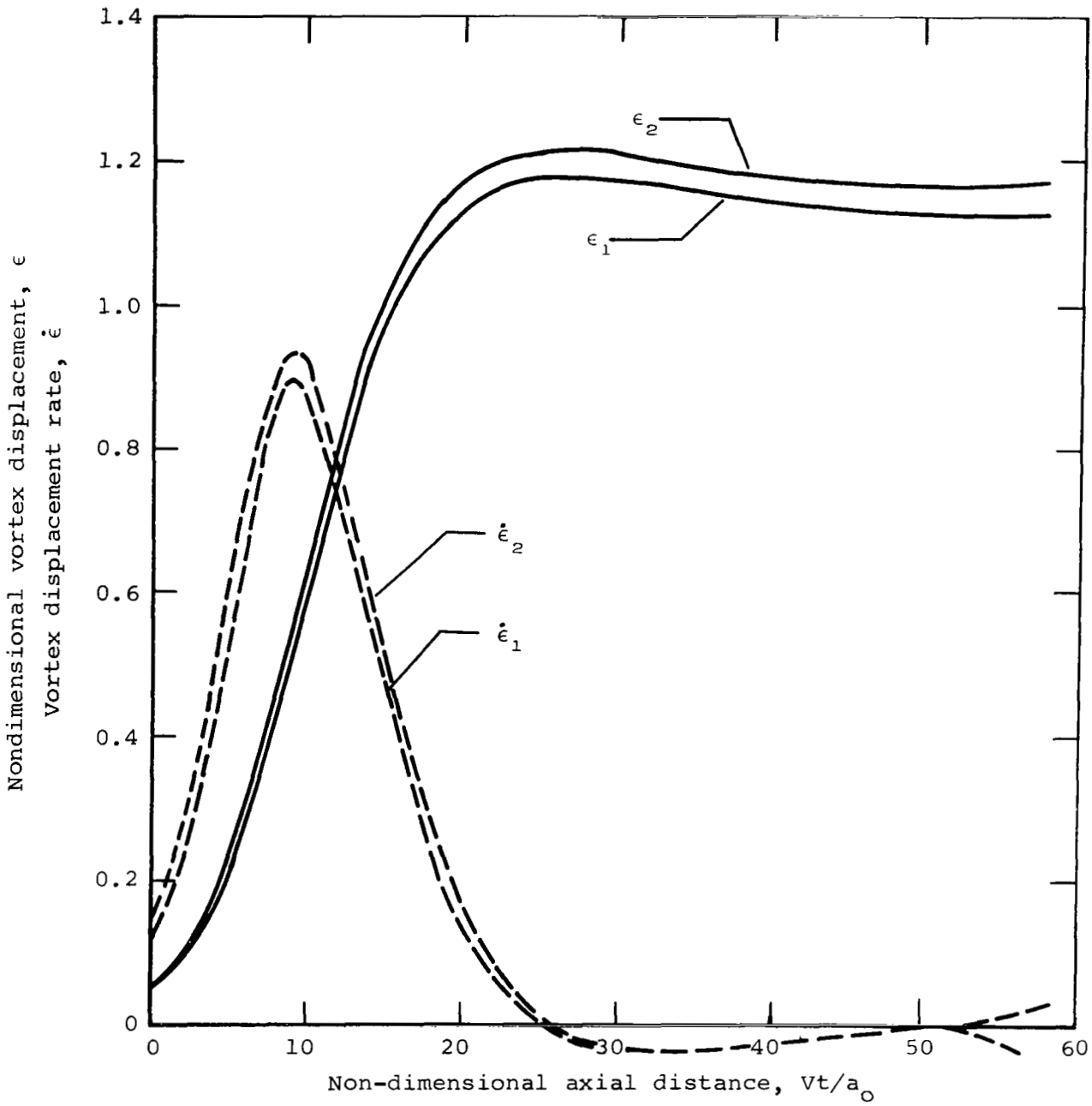

(b) Vortex displacement and displacement rate.

Figure 8.- Concluded

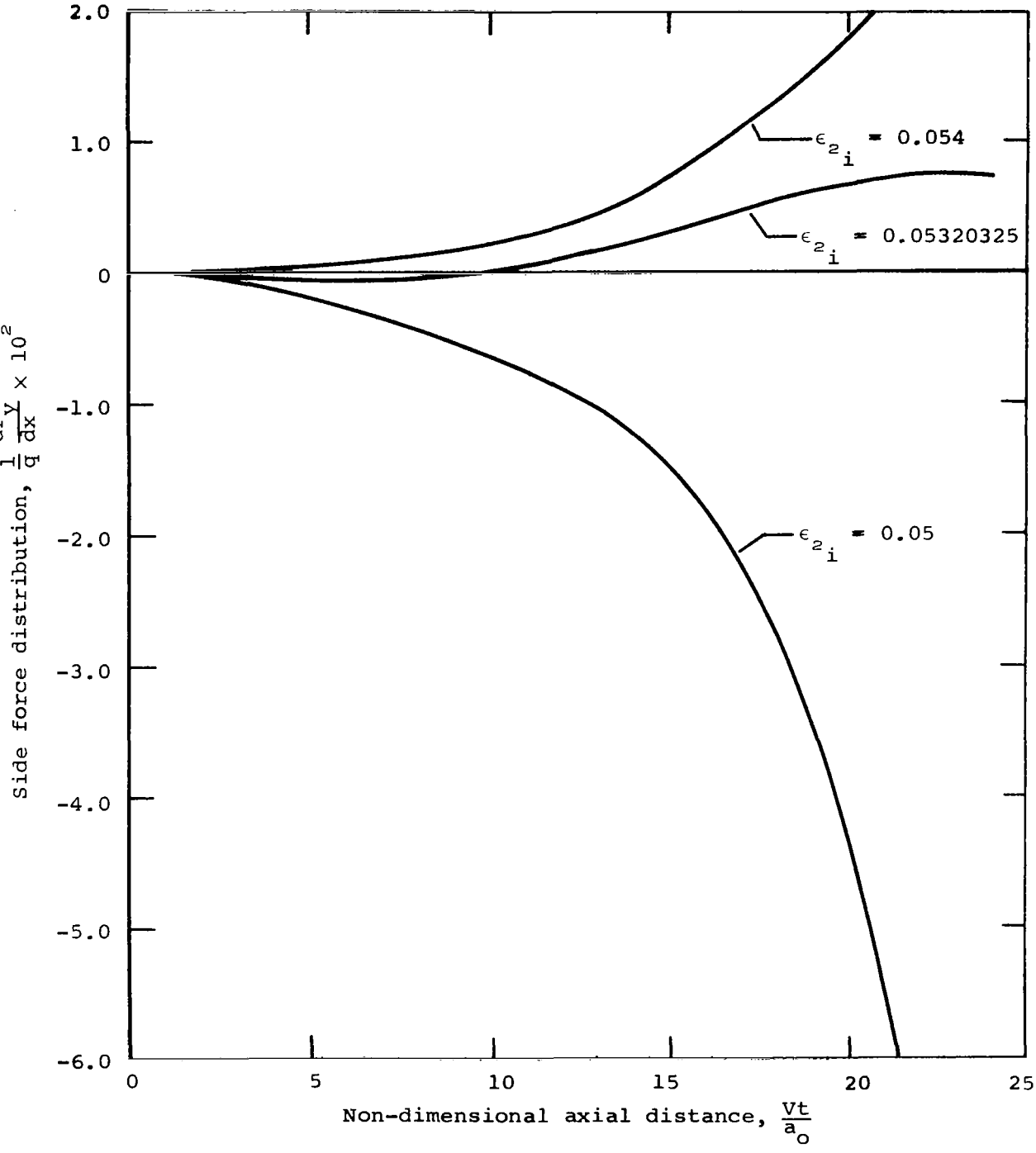

Figure 9.- Theoretical vortex-induced side forces on a cylindrical body for three different initial conditions.

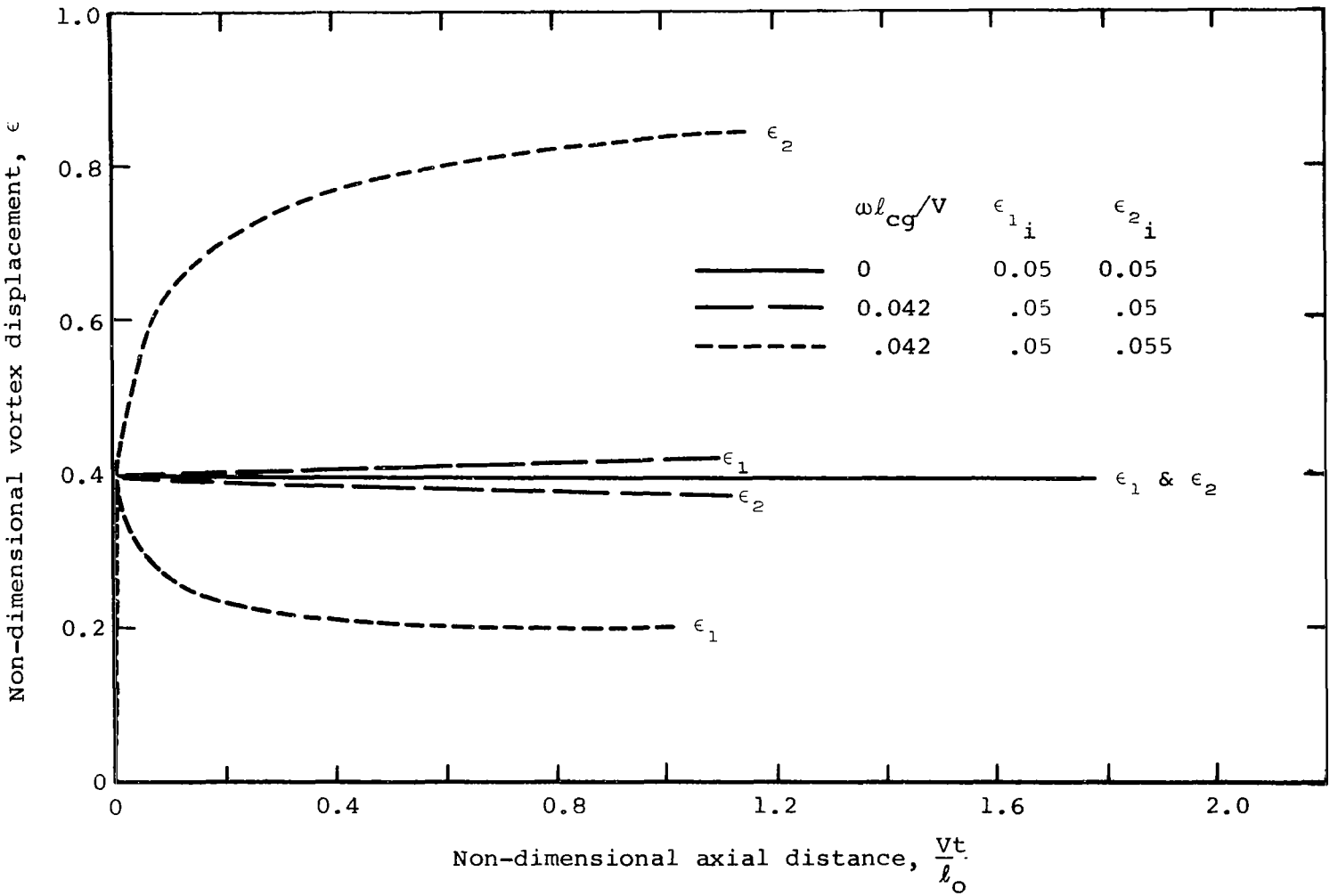

Figure 10.- Non-dimensional vortex displacement on a 10^{o} half-angle cone at 34^{o} angle of attack; feeding points at 34^{o} from resultant crossflow vector.

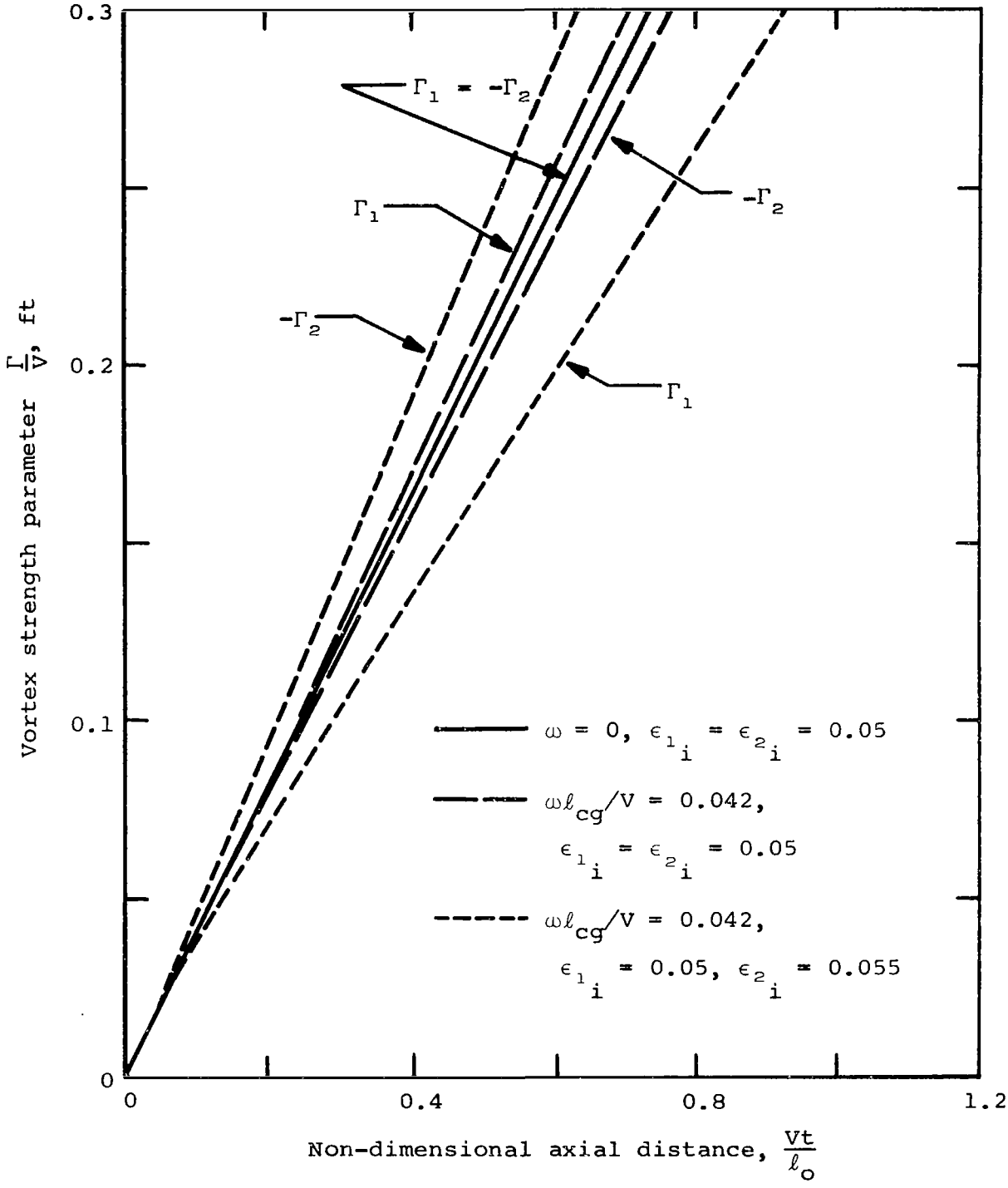

Figure 11.- Variation of vortex strengths for planar and coning motion of a 10° half-angle cone at 34° angle of attack; feeding points 34° from resultant crossflow vector.

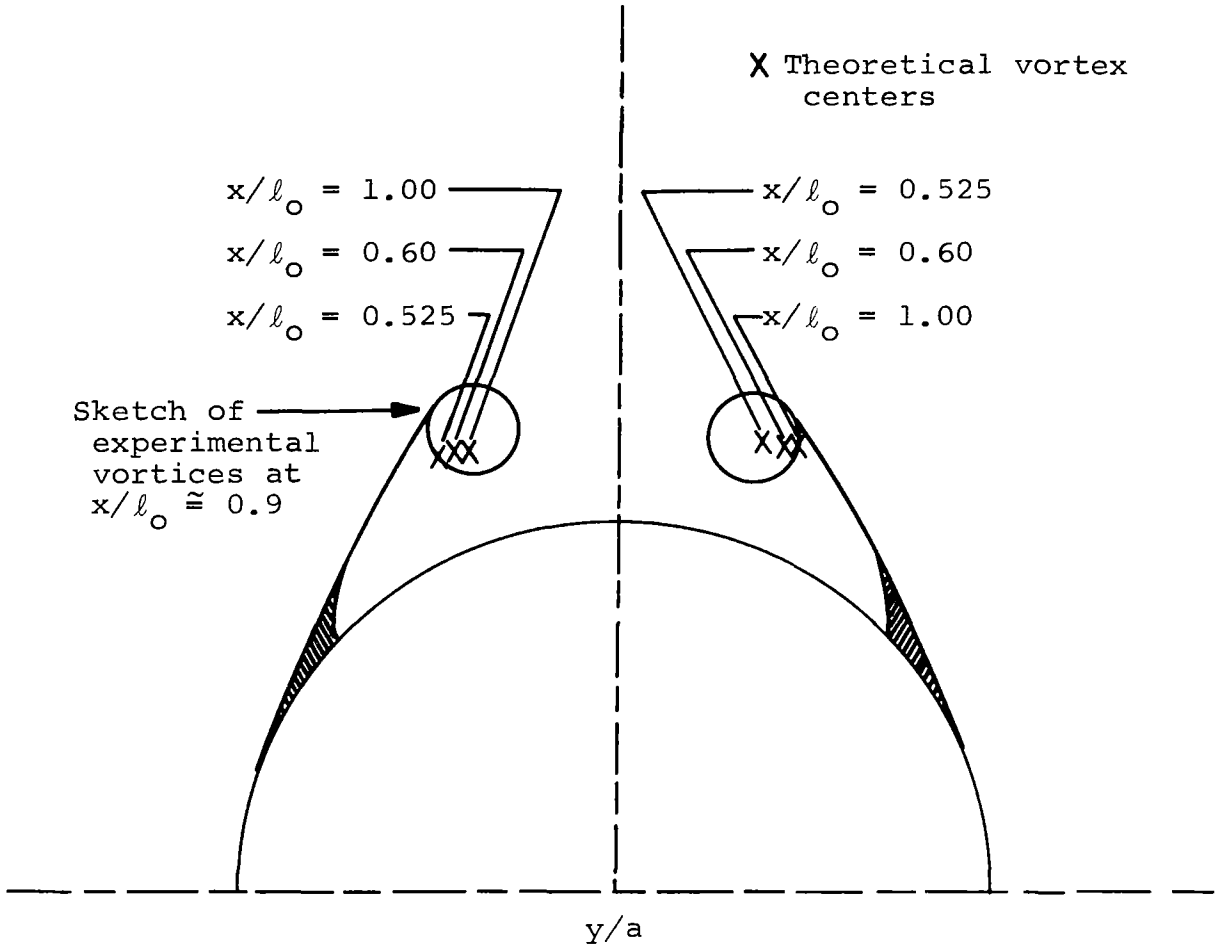

Figure 12.- Comparison of theoretical and experimental vortex trajectories on a 10^o half-angle cone, $\omega\ell_{cg}/V = 0.042$ at 30^o angle of attack.

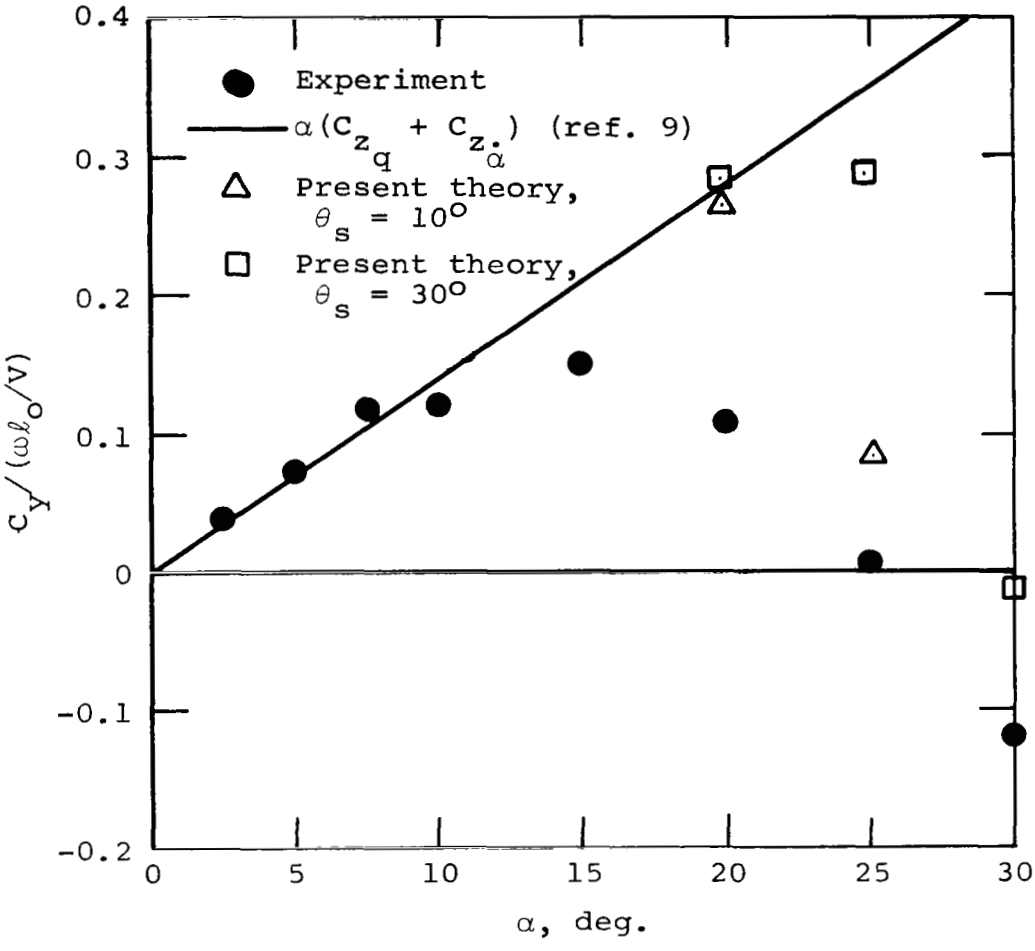

Figure 13.- Side-force coefficient on 10^o half-angle cone due to coning motion; $M_\infty = 2.0$, $\ell_{cg}/\ell_o = 0.61$.

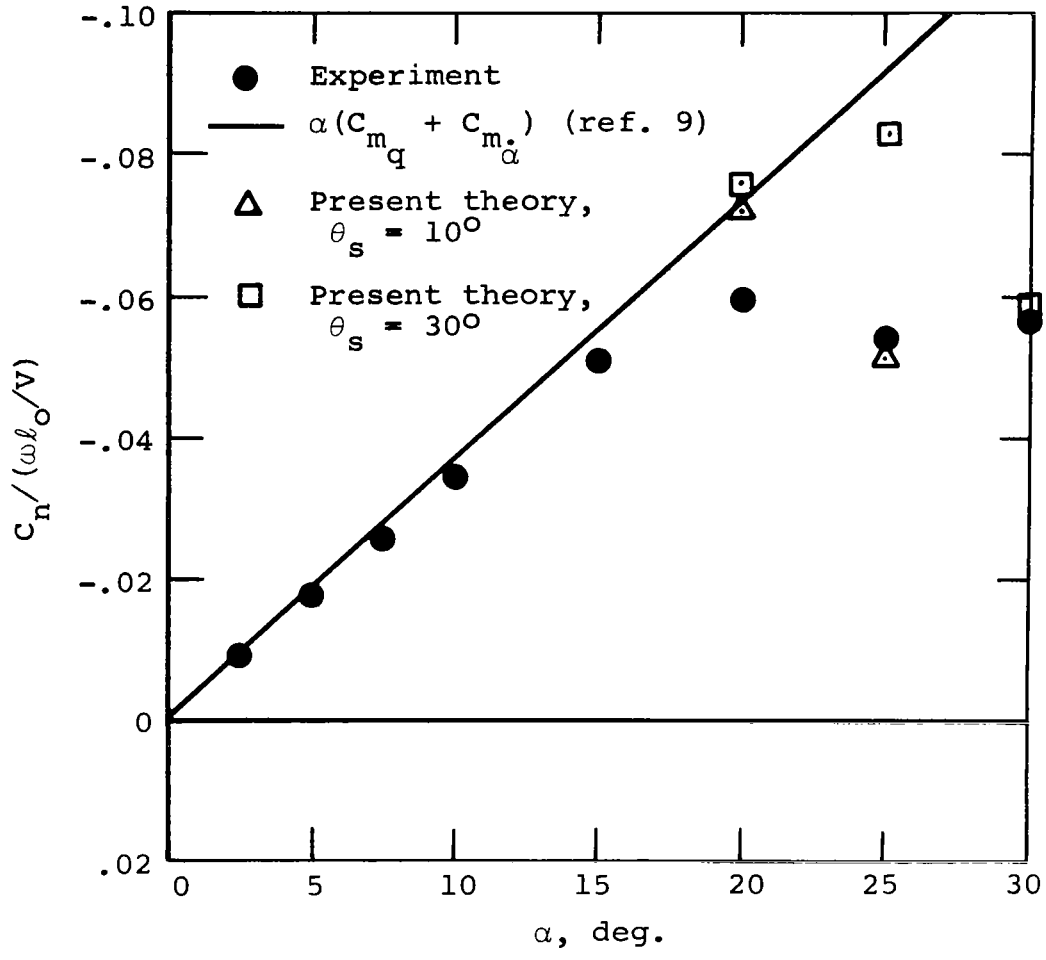

Figure 14.- Side-moment coefficient on 10^o half-angle cone due to coning motion; $M_\infty = 2.0$, $\ell_{cg}/\ell_o = 0.61$.

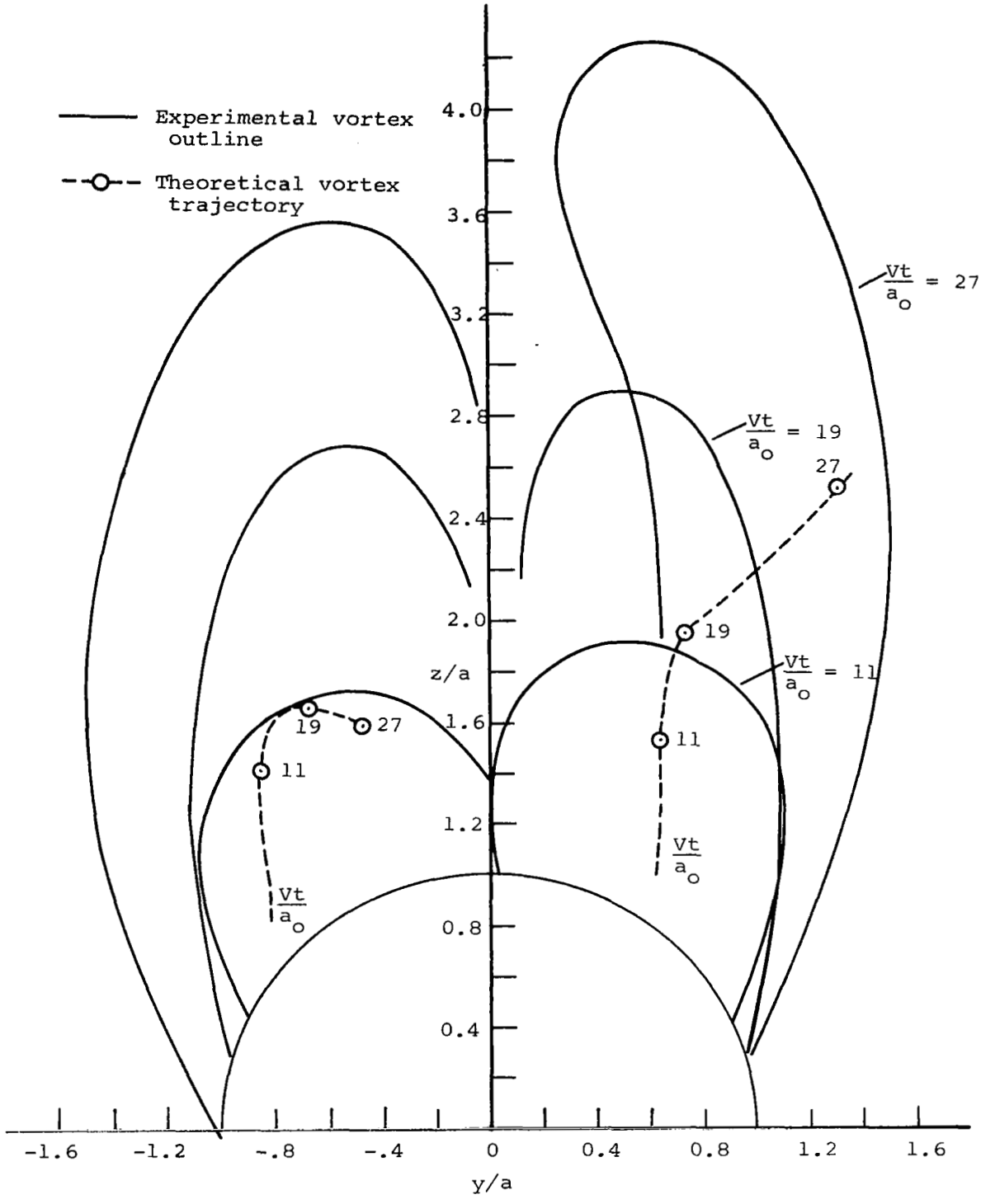

Figure 15.- Comparison of theoretical and experimental vortex trajectories on an ogive-cylinder body in coning motion; $\omega \ell_{cg}/V = 0.12$, $\alpha = 26^{o}$.

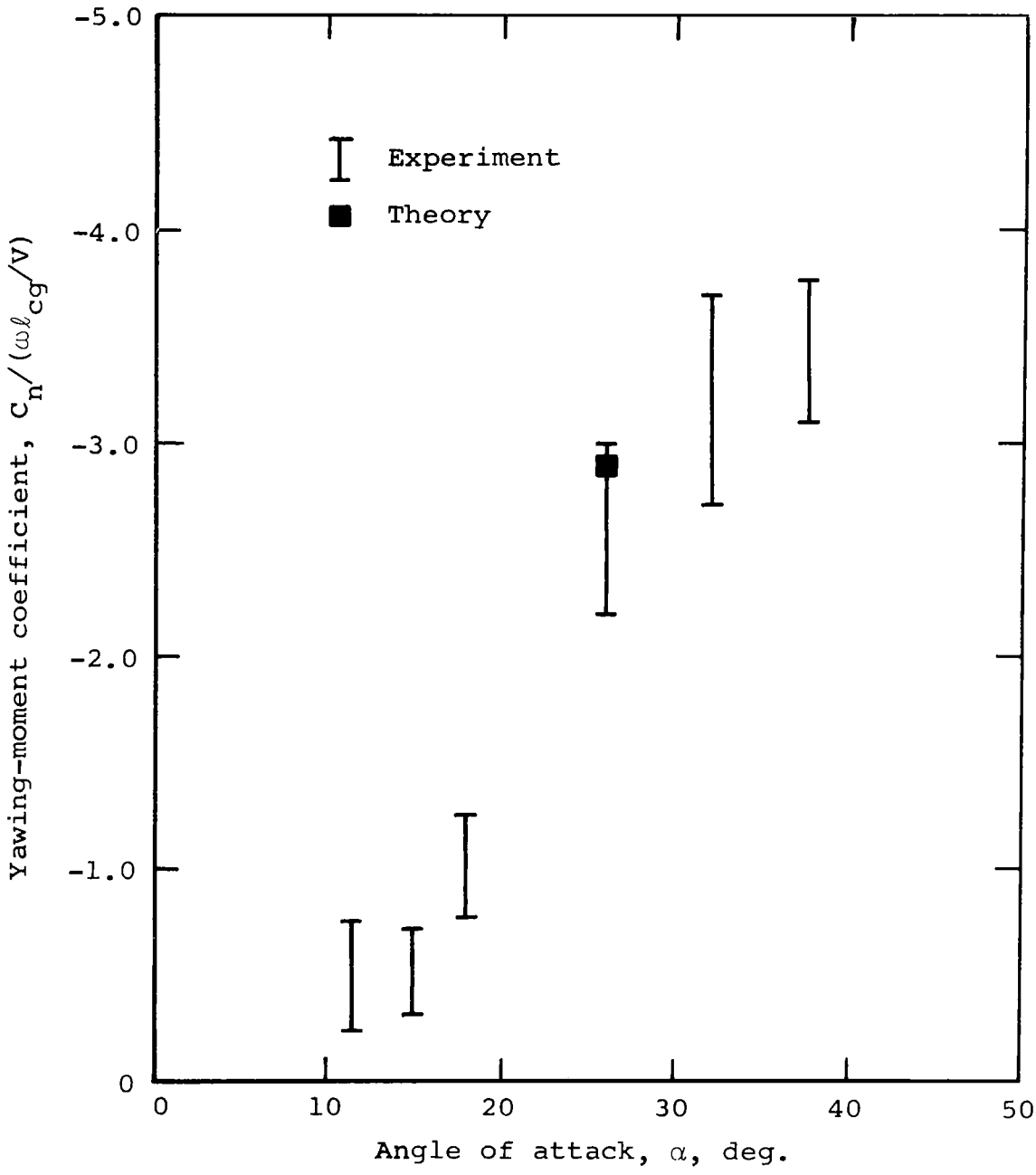

Figure 16.- Side-moment coefficient on a slender ogive-cylinder.

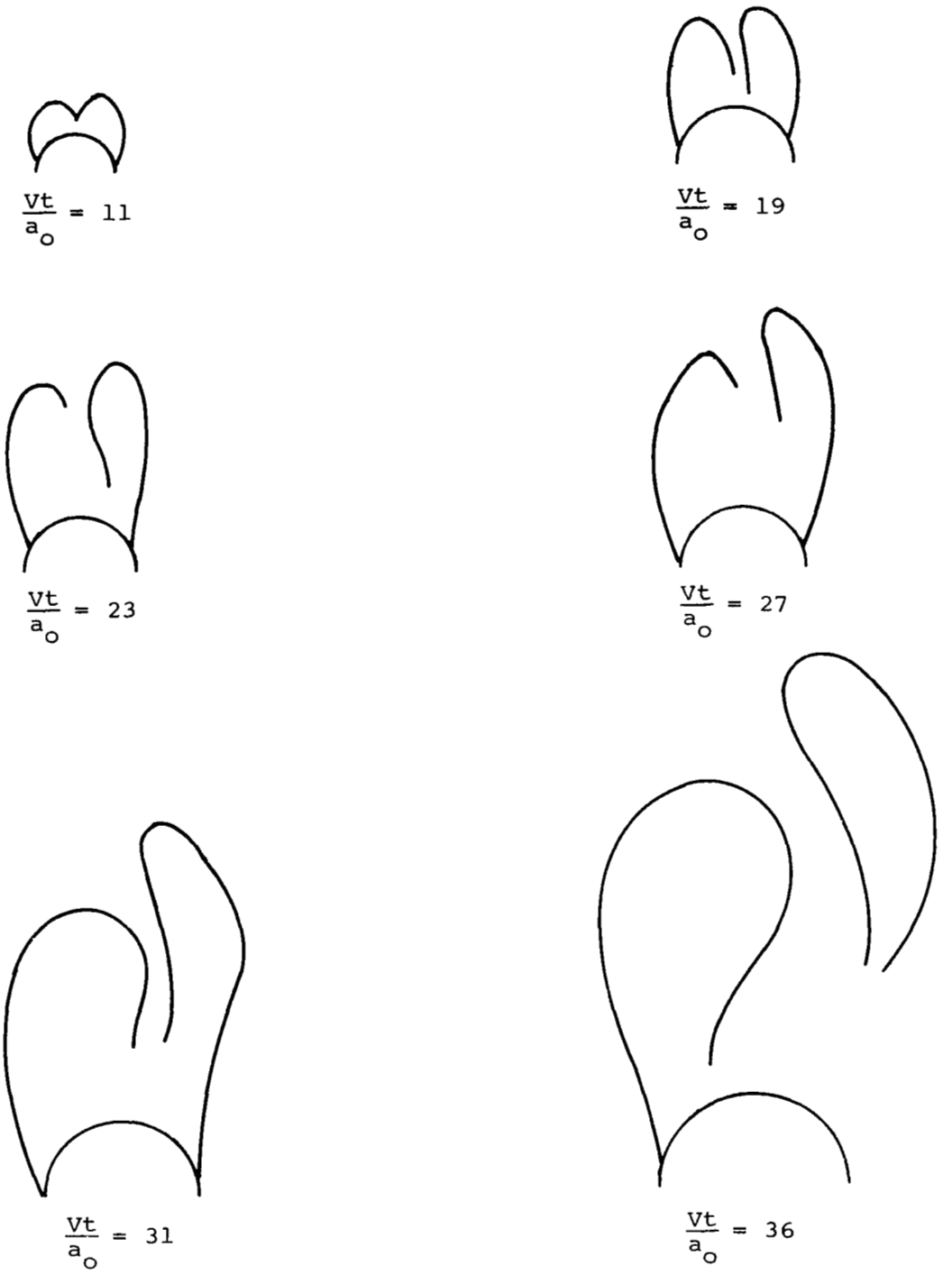

Figure 17.- Sketches of vortices on ogive-cylinder in coning motion from vapor screen photographs, $\omega \ell_{cg}/V = 0.12$, $\alpha = 25^{o}$.

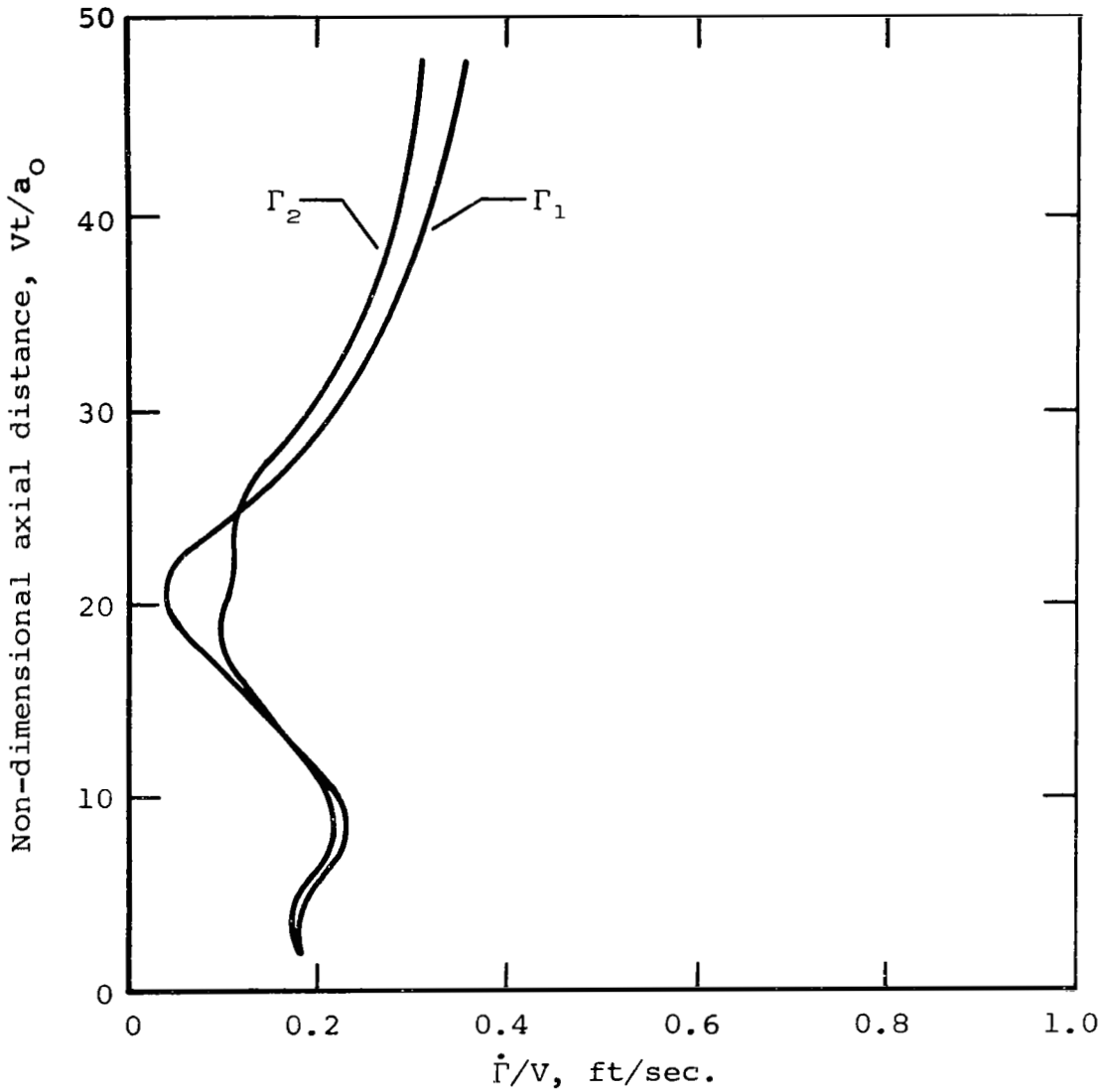

Figure 18.- Variation of rate of change of vortex strength on ogive cylinder, $\omega \ell_{cg}/V = 0.12$, $\alpha = 26^{o}$.